UC San Diego
UC San Diego Electronic Theses and Dissertations

Title

Homodyne target tracking for direct drive laser inertial fusion

Permalink

https://escholarship.org/uc/item/1mt0w075

Author

Spalding, Jon David

Publication Date

2009

Peer reviewed|Thesis/dissertation

UNIVERSITY OF CALIFORNIA, SAN DIEGO

Homodyne Target Tracking for Direct Drive Laser Inertial Fusion

A Thesis submitted in partial satisfaction of the requirements for the degree
Master of Science

in

Engineering Sciences (Engineering Physics)

by

Jon David Spalding

Committee in charge:

    Professor Mark Tillack, Chair
    Professor Farhat Beg
    Professor René Raffray

2009

The Thesis of Jon David Spalding is approved and it is acceptable in quality and
form for publication on microfilm and electronically:

_____

_____

_____
Chair

University of California, San Diego

2009

DEDICATION

This is dedicated to all the people working to bring the dream of clean fusion power to life; who persevere through noncommittal funding, political lack of vision, and their own doubts about the technology itself.

EPIGRAPH

I've very often made mistakes in my physics by thinking the theory isn't as good as it really is, thinking that there are lots of complications that are going on to spoil it—an attitude that anything can happen, in spite of what you're pretty sure should happen.

R. P. Feynman

I've very often made mistakes in my physics, and in my experiments. I think most of my time is spent fixing my errors! 2 steps forwards, 1 step backwards…

J. D. Spalding

TABLE OF CONTENTS

LIST OF FIGURES

ACKNOWLEDGEMENTS

Two papers figures and data with this thesis: J. Spalding, et. al. "Longitudinal Tracking of Direct Drive Inertial Fusion Targets," *Fusion Science and Technology* **52**, *No. 3*, 435-439 and J. Spalding, et. al. "Demonstration of a System for Tracking Direct Drive IFE Targets" (in press). The thesis author was the primary investigator and author of both papers.

ABSTRACT OF THE THESIS

Homodyne Target Tracking for
Direct Drive Laser Inertial Fusion

by

Jon David Spalding

Master of Science in Engineering Sciences (Engineering Physics)

University of California, San Diego, 2009

Professor Mark Tillack, Chair

Direct drive inertial fusion energy (IFE) requires the injection, tracking, and engagement (illumination with high-powered lasers) of reflective spherical shells (targets) in order to produce fusion ignition and energy gain. Targets need to be tracked with 10-µm precision for this method of IFE to succeed. In this paper, one method for tracking targets is investigated, including a brief overview of existing tracking technology, analytical investigation of precision and design, and the results of a small-scale laboratory demonstration. This homodyne displacement measuring interferometer technique is labeled "fringe counting," and although the laboratory demonstration had mixed results, fringe counting may be capable of providing 10-micron precision measurements of target motion along the direction of travel for IFE.

Robustness of the system is a serious concern. Suggestions for future improvement are provided. The conclusion includes an initial design for a full scale IFE

fringe count system that incorporates many of the suggested improvements from this thesis.

In addition to the main body material, several appendices are included. One examines potential for larger-scale injection/tracking demonstrations; another examines the Cat's eye retro-reflector and its invaluable use as an alignment tool for interferometers. And finally, a heterodyne system based on the concept of Zeeman splitting is investigated.

1. INTRODUCTION

This project is a part of the High Average Power Laser (HAPL) program, whose aim is to develop a working direct drive inertial fusion reactor (Sethian). HAPL's efforts entail using results from direct drive inertial confinement fusion experiments, as well has the various laser programs, to compose an integrated power plant design; developments in all the related areas eventually impact the others. For instance, if the physics of ICF implosions is improved and made more robust, this may then reduce the target tracking requirements. Another example is the Glint system that may significantly, if not completely, reduce the need for the fringe count system. Since the future is unknown, this project was pursued with the worst-case scenario in mind.

For direct drive inertial fusion, high power short pulse lasers directly illuminate the surface of a cryogenic Deuterium-Tritium target to cause an implosion that initiates a thermonuclear burn. This implosion is repeated several times per second within a chamber that recovers excess energy from the fusion reaction for generating electricity (see figure 1.1). In order for such a nuclear reactor to function, the lasers that illuminate the target must be aimed with very high precision. Before the lasers can be aimed, the target location must be known—indicating the need for a very high precision, high speed tracking system.

The target itself is specified as an approximately 4-mm diameter, <1% out of round[*], reflective metal-coated sphere of cryogenically frozen D-T fuel (Tillack, Goodin and Alexander). It will be shot vertically into the center of a vacuum chamber of radius 10 m at a speed up to 100 m/s, with aim better than ~5 mm. Total target tracking

---

[*] less than 1% variation in radius over 4π steradians

accuracy needs to be 10 μm in the vertical (z) direction, and 10 μm in each horizontal direction (Petzoldt, Alexander and Carlson).

To this point, no system has been developed to continuously track targets under these circumstances and with this precision[*]. Thus the goal of this paper is to summarize recent research as well as provide a basis for further study. The analysis and demonstrations performed may be relevant for any system based on pointing a coherent light source along the vertical (z) axis to determine z position or velocity; however the focus here is "fringe counting.
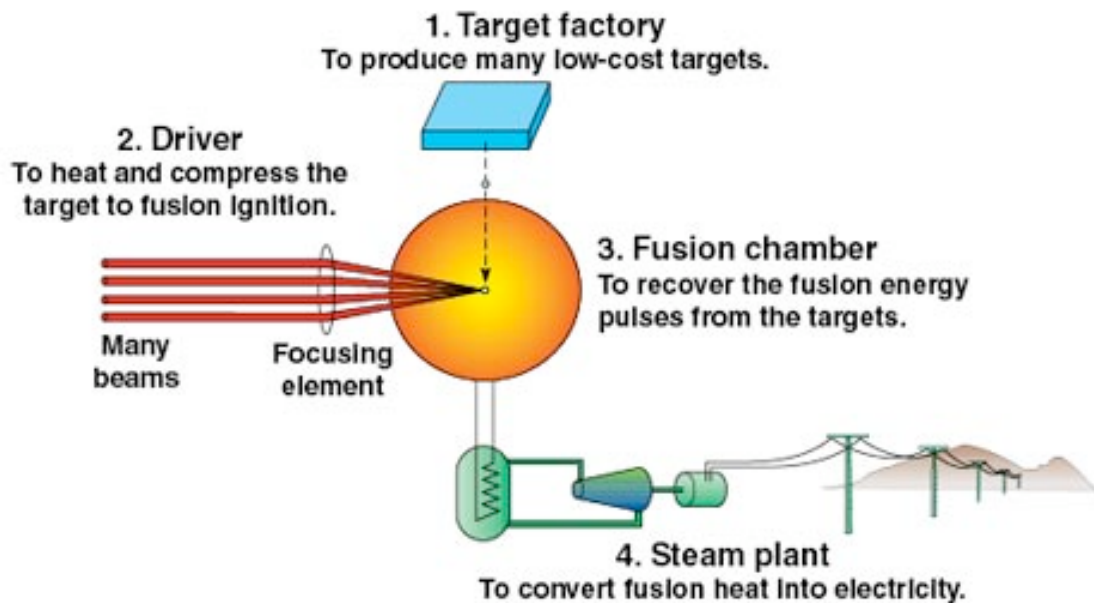
Figure 1.1: Cartoon representation of the workings of an IFE power plant (Lawrence Livermore National Laboratory). *The topic of this paper is indicated in the cartoon by the dashed arrow leading from the target factory to the center of the fusion chamber; specifically, tracking the fusion fuel target as it travels into the chamber. Note that the target is injected vertically downwards, a fact that is important to tracking since the target trajectory is a straight line.*

---

[*] Crossing sensors can be highly precise and will likely play a role in IFE tracking; whether they can beat fringe counting's precision and information content is another matter. Also, fringe counting requires only one laser/receiver port.

At its simplest, fringe counting is a method of tracking an object that is traveling in one direction only. It is the operation of a Michelson interferometer, with a mechanism for recording the total number of interference fringes that pass a stationary detector. A most basic fringe counting system detects rising edges of an electronic signal, and is limited to a precision of ½ the wavelength (λ) of light used; the total count $C \cong 2Z/\lambda$, where Z is the net displacement. A full treatment reveals negligible higher-order corrections; this is covered in section 2, which is devoted purely to the analysis and design of a proposed tracking system.

Section 3 covers a preliminary demonstration of fringe counting, including a novel reference sensor and target dropping mechanism. But before delving into these details, it is worthwhile to briefly overview some other optical tracking systems, and to show how this particular application compares to other types of systems.

1.1. Introduction to Optical Tracking Systems

The most precise measurement systems ever devised are variations of Michelson interferometers; for instance, gravitational wave detectors are designed to measure approximately 10^{-22} strains in spacetime, observed as a 10^{-19} m change in the 4 km interferometer arms. These large machines, besides having some of the largest high-vacuum systems in the world, have very advanced feedback-controlled laser stabilization systems and a variety of methods for filtering signal from noise. Each arm of the interferometer is actually a partially transmitting Fabry-Perot cavity that recycles light, to effectively multiply the light path length and further increase sensitivity. Gravitational interferometers are limited by seismic, shot, and thermal noise (i.e. thermal fluctuations

in mirrors!). The interferometer arms are enclosed in evacuated tubes to reduce noise

caused by gas particles. Figure 1.2 is adapted from (LIGO Scientific Collaboration) and

illustrates the complexity of the system. Bandwidth is in the kHz range.
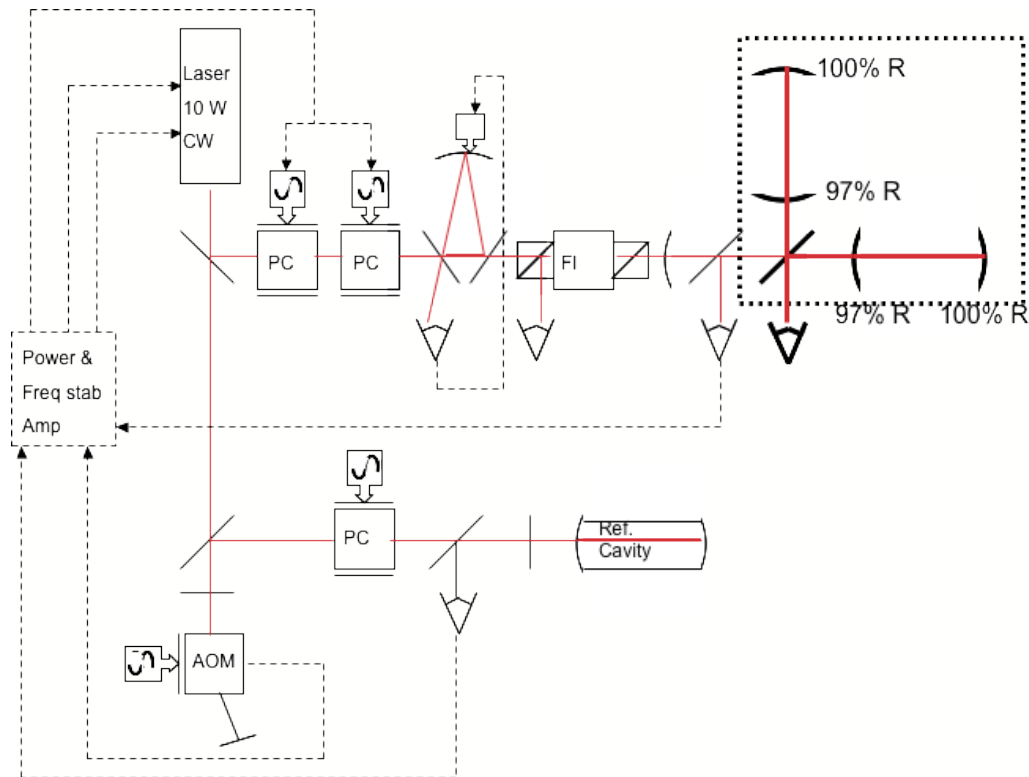
Figure 1.2: A rough representation of LIGO's complexity, derived from (LIGO
Scientific Collaboration)*. PC stands for Pockels Cell, AOM for Acousto-optic modulator,
and FI for Faraday Isolator. The laser itself has at least 3 feedback control signals; two
for laser frequency, and one for laser power output. The bold section is the actual
interferometer; curved mirrors provide multiple passes for each photon so that the
effective light storage time is greater, which effectively increases the size of the
interferometer. The Pockels cells are used to modulate the laser intensity—sidebands are
introduced as a diagnostic. The Faraday isolator prevents light from re-entering and
disrupting the laser. The triangular cavity next to the two pockels cells is used to remove
unwanted sidebands from the laser. The reference cavity on the lower right, combined
with the Acousto-optic modulator, is used to observe tidal strains in spacetime. The
mirrors in the interferometer double as test masses; they are hung as pendulums with a
resonant frequency of 1 Hz, and incorporate magnetic isolators to remove ground
vibration.*

(LIGO Scientific Collaboration) is a valuable source for details on interferometer

design, vibration isolation, laser stabilization, and vacuum technology as relates to the

complex, highly precise, and physically large gravitational wave detectors in operation in the United States.

Commercial interferometer systems, like those presented in (Zygo Company), can measure 0.1 nm displacements with up to 4 m/s velocity at distances up to 10 m (not all with the same system). These rely on the placement of high-quality mirrors or retro-reflectors onto moving surfaces, along with careful alignments. Homodyne systems use a single frequency of light in both reference and measurement legs of the interferometer and can operate independent of laser polarization. Heterodyne systems, in which the reference leg has a different frequency of light than the measurement leg, require use of a dual-frequency laser source. This can come in the form of a Zeeman-laser or acousto-optic modulated laser. In the Zeeman-laser, a magnetic field parallel to the laser output axis causes line splitting—where the two lines have opposite, circular polarization (figure 1.3) (Zygo Company) (Hariharan). In an acousto-optic system, such as with a Bragg cell, the laser output is split into two polarized beams with rotated polarization and a frequency shift. With both methods, the frequency split can be controlled in real-time.

Commercial interferometer systems are limited primarily by speed of electronics and are essentially elaborate fringe-counting systems. Heterodyne systems are usually preferable to Homodyne as they are less sensitive to laser intensity noise and can easily differentiate between forwards and backwards motion (Zygo Company). Homodyne was pursued for this application due to ease of construction, but signal/noise level has been a serious issue (see section 3); at present it is assumed that a heterodyne system could be an improvement over a homodyne system.

The difference between a homodyne and heterodyne fringe count system is that in the heterodyne system, the counting rate is non-zero when the target is not moving. This means one can measure the velocity as a side band impressed upon the non-zero fringe signal. See A.4 for some ideas on implementing a heterodyne system.

LIDAR (Laser RADAR) systems reflect chirped frequency pulses off of a target, which are combined with reference pulses to determine time of flight of the laser pulse and/or Doppler shift. These systems can only operate when the target creates a diffuse reflection (i.e. the surface is rough) or use a retro-reflector (a mirror acts as a retro-reflector if aligned properly), in order that enough light is assured to return to the detector. These seem to be limited to about 1cm/s and 1 cm precision (Pierrottet) in velocity and position, respectively, but have very high velocity and absolute distance measurement abilities, and can even detect velocity and position independently with a single receiver in a single measurement. The factors limiting these systems include speed of electronic processing systems, ability to precisely chirp the laser frequency (i.e. have laser frequency precisely fit a prescribed function in time), and maximum laser intensity (from safety or laser power limitations).
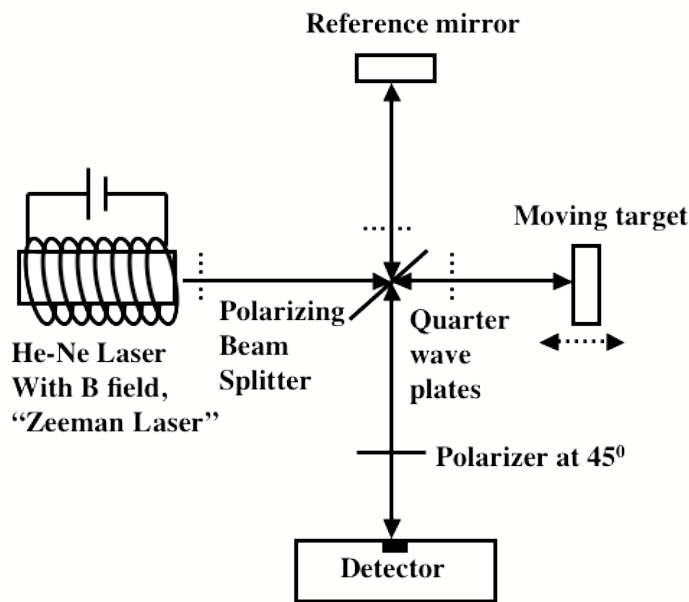
Figure 1.3: A heterodyne interferometer making use of a Zeeman laser. A magnetic field induces a Helium Neon laser to generate dual output: two oppositely polarized, circular polarization waves with a slight shift in frequency (4 MHz according to (Dahlquist, Peterson and Culshaw)*). A quarter wave plate linearizes the polarizations, which are separated at a polarizing beam splitter, and reflected from respective targets. Two more quarter wave plates rotate the polarizations so that both beams arrive at the detector where they interfere, generating a beat signal with frequency equal to the Zeeman shift if the targets have no relative motion. The beat frequency shifts due to the Doppler effect if one target is moving, resulting in a method for measuring target velocity. The Zeeman laser can be replaced with a regular laser followed by an Acousto-optic modulator, which can provide up to a 20 MHz frequency shift. Target velocity information is then stored in the beat frequency.*

LIDAR is commonly applied to atmospheric remote sensing, as the light reflected from atmospheric gases/particles is diffuse. Included in the general category of "LIDAR" is the simple concept of directly timing the arrival of photons after reflection from a target—single photons can provide adequate information for sub-1-cm precision measurements (Murphy). Lidar is conceptually (and perhaps physically) the simplest and most robust optical tracking approach (figure 1.4).

Yet another optical tracking system is VISAR (velocity interferometer system for any reflector) (Barker and Hollenback, Laser Interferometer for Measuring High

Velocities of any Reflecting Surface) (Barker and Hollenback, Laser Interferometer for

Measuring High Velocities of any Reflecting Surface). These systems are used primarily

for measuring velocities and accelerations of extremely high-speed phenomena, such as

shock timing in ICF capsules (Munro and al.) (in this case, shocked D2 becomes highly

reflective). VISAR's reflect laser light from a target surface, and then interfere the

collected light with itself after imposing a temporal delay to one of the signals; typical

velocities measured in (Barker and Hollenbach, Shock-Wave Studies of PMMA, Fused

Silica, and Sapphire) were on the order of km/s, and accelerations of 106 m/s^2.
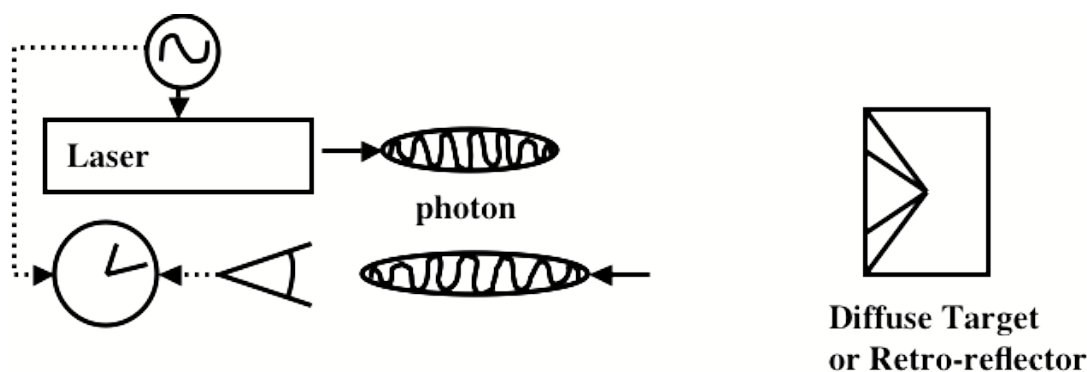
Figure 1.4: Cartoon representation of LIDAR in which a laser outputs pulses of light that reflect from a target and arrive at a detector. Doppler shift and time of flight are used to determine target position and velocity. A function generator is used to impress a sideband modulation onto the laser frequency to make precise measurements possible (for example, see (Pierrottet) *or* (Kubota, Nara and Yshino)*).*

Variations in relative phase over time result in temporal fringes that are then

recorded and analyzed post-experiment (in (Munro and al.), a streak camera displayed the

fringes visually). Precisions of measurements have been around 1-2% (Pierrottet). These

systems tend to be useful only for surfaces that are nearly perpendicular to the laser (such

that much light is reflected directly back to the transceiver), and for motion that is uni-

directional. VISAR is rooted in the WAMI (wide angle Michelson interferometer—see

figure 1.5) concept, in which wavefront aberrations have little impact on quality of

interference. This concept is attractive for tracking IFE targets, except for the crucial fact

that excessive delay times are needed to achieve the desired precision during the coasting

phase of injection. VISAR may be useful as a diagnostic for injector development, where

high accelerations are present; the systems have been used as artillery cannon diagnostics

in the past (Barker and Hollenback, Laser Interferometer for Measuring High Velocities

of any Reflecting Surface). The equation relating velocity to signal frequency for VISAR

is

$$u(t) = \frac{\lambda}{2\tau} F(t)$$

where τ is the interferometer delay time, u is target velocity, and F is the fringe count, *not*

fringe frequency (derived from (Barker and Hollenbach, Shock-Wave Studies of PMMA,

Fused Silica, and Sapphire)). If velocity is constant, then F is also constant—so this

system only works for accelerating targets. For gravitation accelerations, τ needs to be on

the order of 1 s, which is unreasonable.

Any one of these optical methods for measuring velocity and position could

potentially apply to IFE, assuming the technology exists to adapt the system to meet the

precision and speed requirements. For instance, light-time-of-flight (LIDAR)

measurements would be useful if a clock were able to provide 30 fs time resolution. The

10 m distance, 100 m/s velocity, 10 μm precision (or equivalently, 10^{-6} to 10^{-4} velocity

precision—see section 2.1), highly reflective, yet spherically-shaped target, real-time data

analysis, and limits on laser intensity due to target heating (and perhaps still further

considerations!) make IFE target tracking a unique application. The conclusions section

outlines solutions to the problems encountered with homodyne fringe counting.
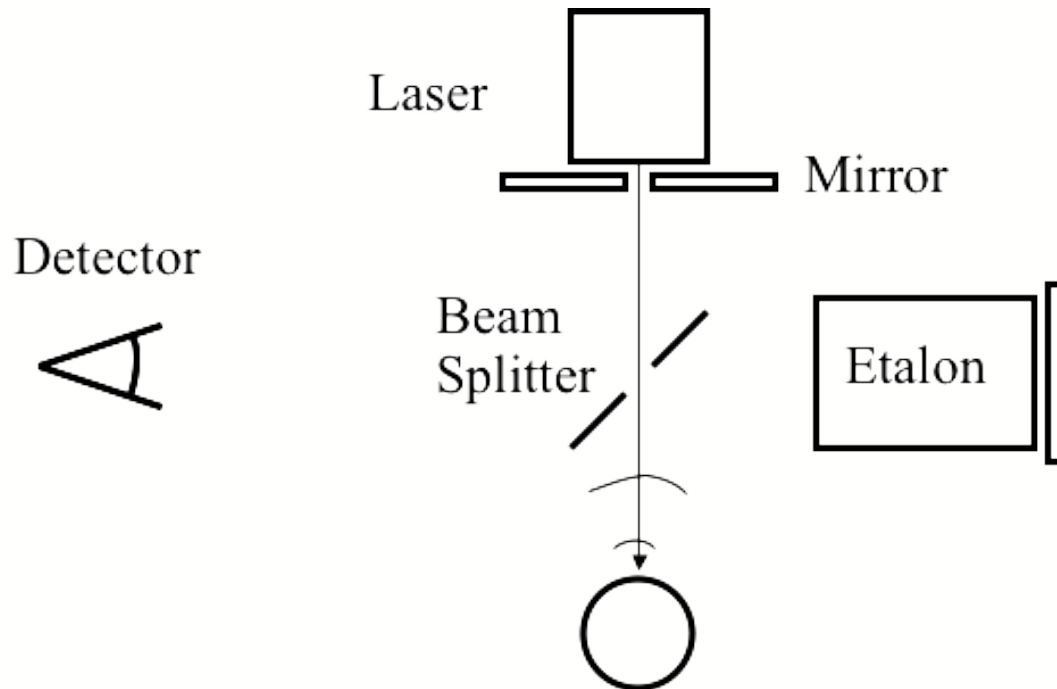
Figure 1.5: Example of a WAMI interferometer, the essence of VISAR—adapted and modified from (Barker and Hollenback, Laser Interferometer for Measuring High Velocities of any Reflecting Surface)*. Light from a source (in this case, the source is the light reflected from a spherical target) is interfered with itself at a detector, where amplitude oscillations indicate changes in target velocity. Two interferometer arms have the same light path length, however the time required for the light to traverse the arms is greatly different. The result is that the wavefront is interfered with itself, with a time delay. This allows the reflecting surface of interest to have an arbitrary shape without hurting signal quality as severely as in a Michelson interferometer.*

2. ANALYSIS AND DESIGN

Analysis, design, optical construction, and literature searches were performed in parallel; this section is placed before the demonstration section for pedagogical reasons.

2.1. Two Scenarios

Two proposed scenarios for the use of fringe counting in inertial fusion are as follows.

In scenario one, a precise crossing sensor provides a reference point near the chamber entrance, from which fringe counting measures target position as a function of time for an entire 10 m distance of travel with sub-10 μm precision. With geometry as indicated in fig. 2.1, the error allowances can be calculated as follows;

Scenario 1

Target Injector

Crossing Sensor;
At $t_{initial}$= -0.1 s $z_{initial}$ = 10 m
And v = -100 m/s

Chamber Center,
At t_{final}= 0 s, z_{final} = 0 m
And v = -101 m/s

Chamber Wall
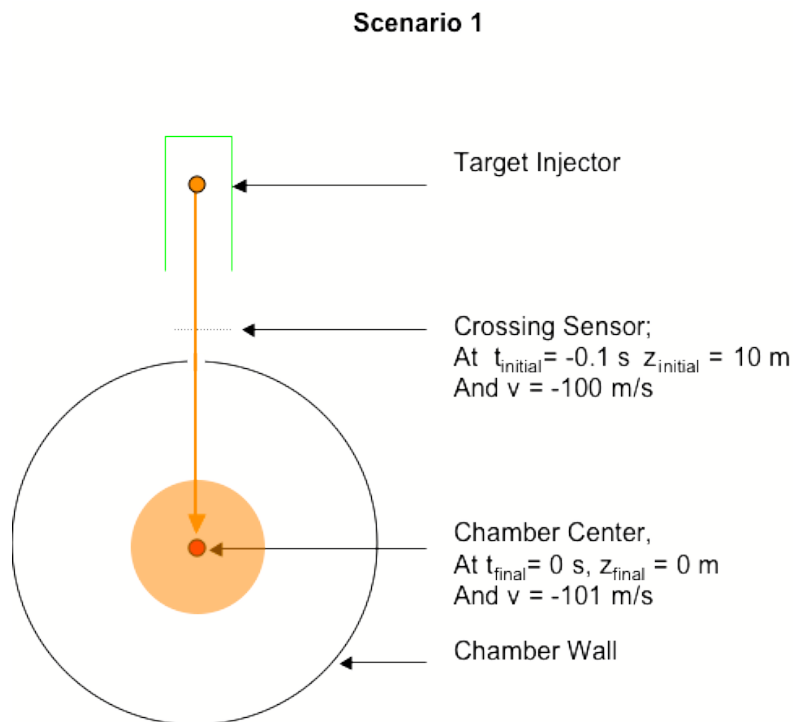
Figure 2.1: Tracking scenario 1, in which the target is tracked for 0.1 s and 10 m as it travels from a crossing sensor near chamber entrance to approximately chamber center. The times, velocities, and positions are approximated for purposes of rough error analysis.

11

$$\delta z_{final} \simeq \sqrt{\delta z_{initial}^{2} + \delta z_{fringe}^{2}}$$

where $\delta z_{initial}$ is the error introduced by the crossing sensor, δz_{fringe} is the error introduced by the fringe counter, and δz_{final} is the final error in measuring target position which must be less than 10 μm. The minimum $\delta z_{initial}$ reported with a crossing sensor is 2.5 μm (Petzoldt and Jonestrask, IFE Target Injection Tracking and Position Prediction Update); this leaves about 9 μm for fringe counting when added in quadrature, i.e. assuming a random distribution of errors. Note that velocity will be well determined under this scenario since a continuous record of target position will be available. Net target position needs to be known to 1 in 10^{6} with this scenario.

Scenario two assumes that the Glint mechanism functions as hoped (Carlson, Tillack and Lorentz) (Carlson, Tillack and Lorentz); the Glint then replaces the crossing sensor, and provides a temporal-spatial reference point for the engagement system. Then fringe counting just provides a precise velocity measurement at z_{glint} to correctly time the drivers (fig. 2. 2).

At the time of this writing, Glint performance isn't available. Assuming an arbitrary Glint longitudinal position error of 7 μm (δz_{glint}) leaves 7 μm (δz_{fringe}) for fringe counting's velocity/laser timing prediction. How many fringes need to be counted to get this kind of timing precision? First, the allowed velocity measurement error at a 10 cm glint standoff (z_{glint}) is found as follows:

Scenario 2

Target Injector

Glint, z_{glint} = 10 cm,
And v_{glint}= -101 m/s, t_{glint}= -1 ms

Camber center
z_{final} = 0 m, t_{final} = 0 s, v_{final} = 101 m/s
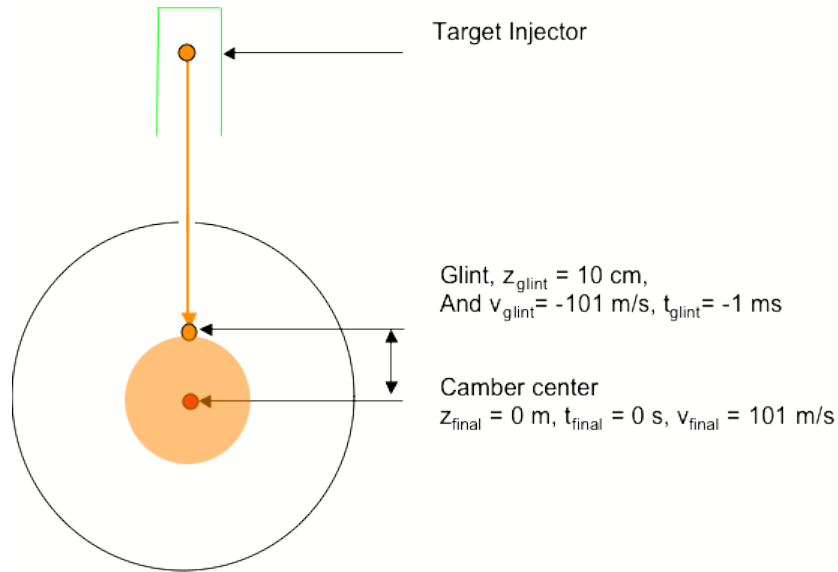
Figure 2.2: Tracking scenario 2, in which the target is tracked for 0. 1 ms and 1 cm at the glint location, z_{glint}, which is 10 cm and 1ms before target engagement. Glint provides a temporal and spatial reference point, but not target velocity; fringe counting can provide target velocity if needed.

$$z = vt \rightarrow \delta z_{final} = \delta v_{fringe} \cdot t_{glint} + v_{fringe} \cdot \delta t_{glint}$$

$$\frac{\delta v_{fringe}}{v_{glint}} = \frac{\delta z_{final}}{z_{glint}} \rightarrow \delta v_{fringe} = \frac{\delta z_{final}}{z_{glint}} \cdot v_{glint}$$

$$= \frac{7 \cdot 10^{-6}\,\text{m}}{0.1\text{m}} \cdot 100\text{m/s} = 7 \cdot 10^{-3}\,\text{m/s}$$

The time error, δt_{glint}, is ignored since it was already taken into account as the glint longitudinal position error. If each interference fringe corresponds to a distance of Δz, which is approximately the resolution of the fringe counter, then

$$\frac{\delta v_{fringe}}{v_{glint}} = \frac{\Delta z}{z_{fringe}} \rightarrow z_{fringe} = \frac{\Delta z \cdot v_{glint}}{\delta v_{fringe}}\,\text{m}$$

$$z_{fringe} \simeq \frac{100\text{m/s} \cdot 1.5\,\mu\text{m}}{7 \cdot 10^{-3}\,\text{m/s}}\,\text{m} = 2\ \text{cm}$$

For fringe counting, Δz is $\sim\lambda$; therefore z_{fringe} is about 2 cm if λ is 1.5 μm. This means that operating the fringe counter at the Glint to collect 2 cm of fringe count data should be enough to get the timing precision needed to engage the target, assuming there is no chamber gas to slow it down. Compare this with the 10 m of fringe count data for continuous measurement, where laser wavelength stability and iris size (covered later) become issues. Of course, if the fringe counter has more error than λ, either a shorter wavelength can be used, or a longer data collection period is required. Note that scenario 1 is advantageous in the case that chamber gas is slowing down the target, since more information is available on target position.

2.2. Doppler Shift and Interference

This section will briefly cover the basics of Doppler shift, plane-wave interference, and how they relate to the fringe counter.

For a light source approaching a detector with velocity v, the wavelength is shifted as follows:

$$\beta = \frac{v}{c}$$
$$\lambda' = \lambda_0 \sqrt{\frac{1-\beta}{1+\beta}}$$

Now, based on relativity, it does not matter whether the detector or the source is moving; the shift measured at the detector will be the same. Since the light leaving the laser is shifted according to an observer on the target, and then upon reflection re-enters

the reference frame of the laser, the Doppler shift actually occurs twice. This results in a

total wavelength shift of:[*]

$$\lambda = \lambda' \sqrt{\frac{1-\beta}{1+\beta}} = \lambda_0 \frac{1-\beta}{1+\beta}$$

For small β, the formula can be approximated by

$$\lambda \simeq \lambda_0 (1-\beta)^2 \simeq \lambda_0 (1-2\beta) .$$

The error using this approximation is of the order of β^2, or parts per trillion.

For the superposition of two monochromatic, planar E/M waves with equal

polarization but wavelength or phase that varies in time (taken at a single, constant z

position):

$$\mathrm{E} = \frac{E}{2} e^{+i(\omega t+\phi)} + \frac{E}{2} e^{-i(\omega t+\phi)} = \frac{A}{2} e^{\pm i(\omega_a t+a)} + \frac{B}{2} e^{\pm i(\omega_b t)}$$

$$\mathrm{I} = \mathrm{E} * \mathrm{E} = \frac{A^2+B^2}{2} + \frac{A^2}{2} \cos(2\omega_a t + 2a) + 2\frac{B^2}{2}\cos(2\omega_b t) + AB\cos\{(\omega_a - \omega_b)t + a\} + AB\cos\{(\omega_a + \omega_b)t + a\}$$

The intensity, I, of the electromagnetic wave is the property being observed, and

is evaluated by multiplying the complex wave function with its complex conjugate. The

three high frequency terms are not of interest. The result is

$$\mathrm{I} = AB\cos\{(\omega_a - \omega_b)t + a\} .$$

Now we can substitute the local oscillator (reference wave) and Doppler shifted

light frequencies to arrive at the final equation:

---

[*] For a target that is traveling away from the detector, simply switch the numerator/denominator in the above relation. If v = 100 m/s, and λ_0=1.5000000 μm, then the shifted wavelength, λ=0.999999333λ_0 = 1.499999000 μm , which is a shift of precisely 2/3 parts per 1 million.

$$\omega_b - \omega_a = \omega_0\left(\frac{1+\beta}{1-\beta} - 1\right) \simeq \omega_0[(1+\beta)^2 - 1] \simeq 2\omega_0\beta = 2\frac{v}{\lambda}$$

$$I_{AC} = AB\cos\left(\frac{2v}{\lambda}t\right)$$

where I_{AC} is the sinusoidal component of the observed light intensity.

A second way of arriving at this result is to think of the frequency of the two waves as remaining constant, but the phase "a" of one wave is advancing as $(2v/\lambda)t$ relative to the other wave. This is a physically inaccurate interpretation[*], but emphasizes the simplicity of this tracking method—it's as if a ruler (with $\lambda/2$ rulings) is attached to the target and dragged passed the counter.

An important fact gleaned from this analysis is that the signal intensity depends not just on the amount of light coming from the target, but also on the amount of light present in the reference leg of the interferometer.

Now let us consider the light travel time, which creates an information delay; the fringe count information is "outdated." If the target is a distance Z from the detector, it will take δt seconds for the position information to arrive at the detector, and the error in position will be δZ meters, assuming that v is constant over δt:[†]

$$\delta t = \frac{Z}{C}$$

$$\delta Z = v\delta t = \frac{vZ}{C}$$

For the case of interest, $\delta Z = 3$ μm. Therefore, light travel time needs to be entered into any position-predicting algorithms in a full-scale IFE plant (this applies to all

---

[*] Just as Newtonian mechanics is a physically inaccurate model of Relativistic mechanics.
[†] v = 100 m/s, Z = 10 m, C = $3*10^8$ m/s; dZ = 3 μm

optical tracking systems). The average shot-to-shot target velocity could be used to add a constant to position/timing algorithms.

2.3. Spherical Wave-fronts

Interferometer-based measuring systems usually use mirror, retro-reflector, or diffuse surfaces; these all generate good fringe contrast. However in this case, the surface of interest is a convex spherical mirror, which is moving in 3 axes. This results in a ringed interference pattern that changes in time.

First, the interference pattern appears as a "bull's eye" when viewed head-on; figure 2.3 represents the formation of the interference pattern, as well as variables used for analyzing interferogram properties.
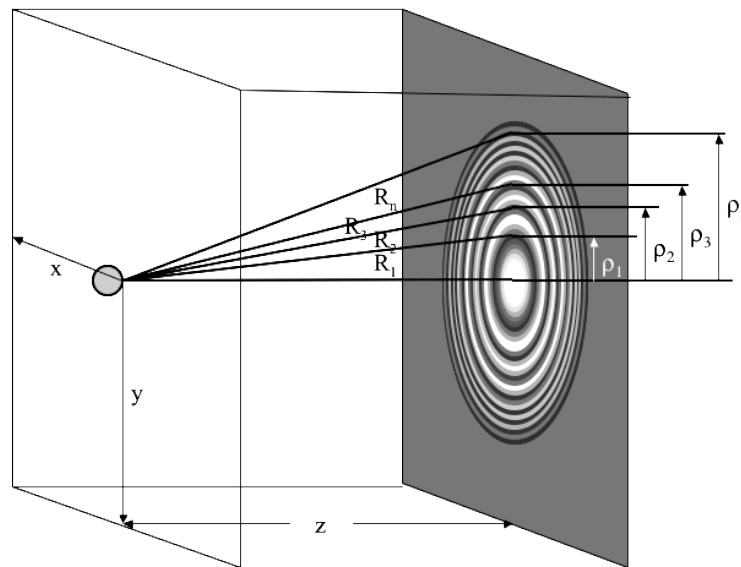
Fig. 2.3: Diagram with variables labeled for calculating properties of interference pattern generated by superimposing planar wavefronts with the reflection from a sphere. R is spherical wavefront path-length to a given point in the interferogram, ρn is the radius of the nth dark fringe which is $(2n+1)\pi/2$ radian phase shift from center of bull's eye, z is distance from imaginary focal plane of sphere to plane of interferogram.[*]

---

[*] The imaginary focal point of a convex spherical mirror is ½ the radius of curvature beyond the front surface. Figure 2.3.1 is deceptive in that it shows light rays converging at the target surface rather than the focal point.

Using properties of right triangles, one can calculate the radii of the nth dark ring (as pictured in fig. 2.3):

$$\rho_n^2 + z^2 = R_n^2$$
$$R_n \equiv (2n-1)\lambda / (2+z)$$
$$\rho_n^2 + z^2 = \left[(2n-1)\lambda / (2+z)\right]^2$$
$$\rho_n = \sqrt{\left[(2n-1)\lambda / (2+z)\right]^2 - z^2}$$

simplified by dropping all terms of order λ^2,

$$\rho_n = \sqrt{(2n-1)\lambda z} \ .$$

The first dark fringe has radius

$$\rho_1 = \sqrt{\lambda z} \ .$$

One can compute the integrated power received from each bright ring in the image plane. First, the area of the nth ring is

$$A_n = \pi(\rho_n)^2 - \pi(\rho_{n-1})^2$$
$$A_n = \pi\lambda z[(2n-1)-(2n-3)]$$
$$A_n = 2\pi\lambda z$$

We have neglected all terms of order λ^2, equivalent to assuming that $z \gg \rho_n \gg \lambda$. If one assumes that the tracking laser beam has a flat intensity profile, as would be desirable, then the integrated intensity of the nth bright fringe is the same for all n (of course, a narrow, Gaussian beam produces much higher intensity at the center).[*]

Therefore, if the detector upon which the interference pattern falls is a photodiode with output that is the integral of the photon flux impinging on its surface, and the radius of the detector is significantly larger than $\sim\rho_1$, the desired AC signal will tend to cancel

---

[*] A flat beam intensity profile keeps the return signal constant when the target wanders off-center

out. This was observed experimentally (even with a Gaussian beam); to optimize signal amplitude, an iris was placed before the detector at radius $\sim\rho_1$ (fig 2.4), while a lens was used to bring the radius down to the size of the photodiode. Lenses have the effect of shrinking the spatial extent of the interference pattern, without impacting integrated intensity.
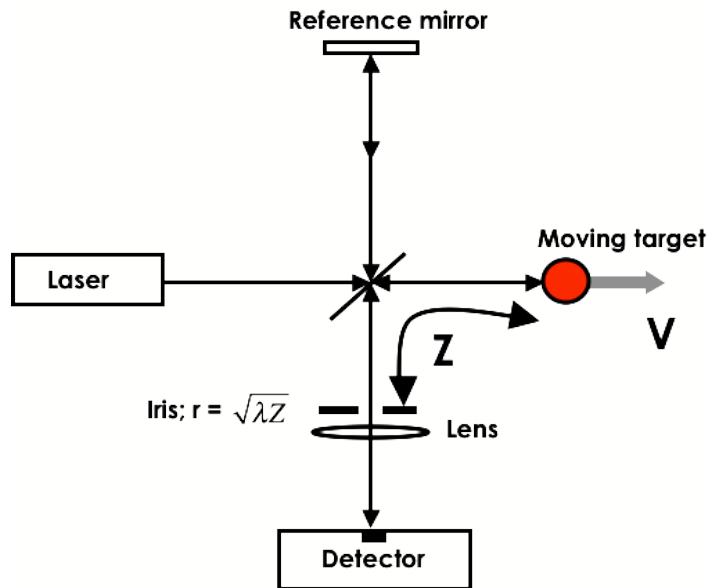
Figure 2.4: Interferometer with iris and lens to focus central interference spot onto detector and obtain maximum signal amplitude. The target is assumed to stay aligned with the iris.

A similar effect results if the iris mentioned above is offset in the x or y axes (fig. 2.5) relative to the sphere.

A rudimentary treatment of the expected losses due purely to offset in x- or y-axis follows, for an iris matched to ρ_1:
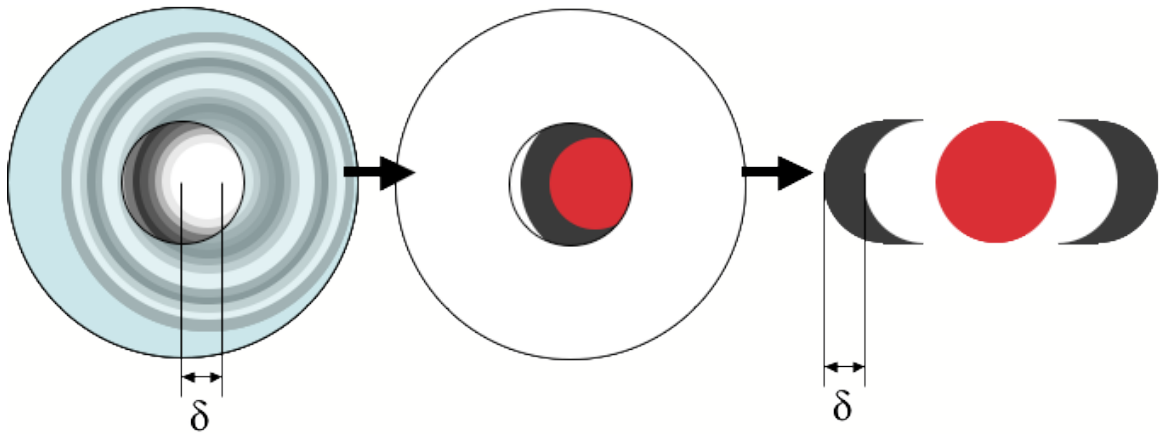
Figure 2.5: The left figure is approximately what the detector will "see" when the target is off center by ~ρ1. The effect was modeled by first assuming that each fringe is either all bright or all dark (red or grey); then the blocked, as well as dark, areas are approximated and subtracted from the bright area. This is represented in the rightmost figure by subtracting the two black areas from the red area.

Using the simple model for offsets presented by fig. 2.5, the net signal amplitude

is (as a fraction of maximum):

$$\text{Fraction} = \frac{\pi\rho_1^2 - 2\delta\rho_1}{\pi\rho_1^2}$$

$$0 = \pi\rho_1 - 2\delta \Rightarrow \delta_{max} \sim \frac{3\rho_1}{2}$$

where δ is the offset, the laser beam has flat intensity profile, and the interference rings

are modeled as a bull's eye (i.e. either all light or all dark). Maximum offset,

corresponding to 0 signal amplitude, occurs with an offset of about $1.5\rho_1$. By the same

analysis, a signal fraction of 0.5 is obtained when δ is about $0.75\ \rho_1$. Experimentally, a

fraction of 0.5 was obtained with an offset of about $0.8\ \rho_1$ (although the actual iris size

was approximate; the iris in use was difficult to measure). Signal filtering/amplification

hardware can potentially compensate for some of these losses. Alternatively, if the iris is

set smaller than ρ_1, a trade-off is made between greater allowable offset and maximum signal strength.

A relevant example is the case of a target at 10 m standoff with 1.5 μm light; ρ_1 = 4 mm, and maximum allowable δ is of order ±3 mm. This is near the proposed performance of target injectors.

Now suppose that the mirror in fig. 2.4 is replaced with a stationary target, of same properties as the moving target (fig. 2.6).
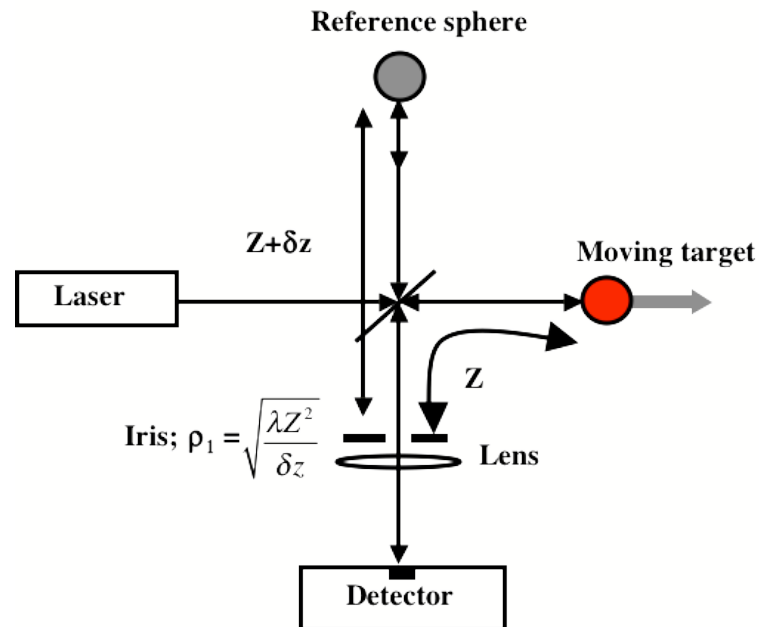
Figure 2.6: Interferometer with a stationary reference sphere and moving target sphere, both with same properties. The interferogram present at the iris plane is very similar to that for the mirror/sphere case (a mirror is a sphere of infinite radius). The formula for ρ_1 in the figure is derived later on.

Analyzing this configuration is useful since it was proposed as a method of combating the problems with spherical wave-fronts covered above; it will apply to the proposed wave-front correction system later on.

It was shown experimentally that two-sphere interference generates near-perfect light or dark unless either the spherical wavefronts are offset by some small amount as in fig. 2.7 (leading to striped patterns), or the two arms of the interferometer have effective differences of path length (leading to bull's eye patterns, figure 2.8). Though it is technically feasible to solve for the full mathematical description of the interference pattern, it is much easier (and likely more useful) to derive some simple geometric arguments to determine interferogram properties.

Figure 2.7: Determining the maximum offset, o, in a sphere-sphere interferometer before more than one-half fringe is present on the detector of diameter D. The spheres could also be represented as point sources of light; the point source would be located at the imaginary focal plane of the sphere, 1/2 a target radius from the center of the target. The second figure illustrates the desired interference intensity across the detector face at an instant in time (one cycle later, the central peak would be a minimum).

First, assume z >> D > o; subtract the difference in hypotenuse for the two right triangles shown in figure 2.7, and set that difference equal to λ/4, then solve for o, which is the maximum offset. In other words, if less than a full fringe is visible on the detector a high-amplitude signal will be detected.

$$z^2 + \frac{D^2}{4} = L^2;$$

$$z^2 + \frac{D^2}{4} + Do + o^2 = (L + \varepsilon)^2;$$

$$L^2 + Do + o^2 = (L + \varepsilon)^2;$$

$$1 + \frac{Do}{L^2} + \frac{o^2}{L^2} = (1 + \frac{\varepsilon}{L})^2 = 1 + \frac{2\varepsilon}{L} + \left(\frac{\varepsilon}{L}\right)^2$$

$$\frac{Do}{L^2} \simeq \frac{2\varepsilon}{L} \Rightarrow o \leq \frac{2\varepsilon L}{D} = \frac{\lambda L}{2D} \simeq \frac{\lambda z}{2D}$$

$$o \leq \frac{\lambda z}{2D}$$

A relevant case is z = 10m, λ=1.5 μm, D = 2 cm, o = 0.375 mm. Since full-scale injectors are expected to perform with o ~ 5 mm, using two spheres like this won't work with a 2 cm wide detector (but a 2 mm detector might).

A similar analysis can be performed for offsets in the Z direction (figure 2.8). In this case, 0 offset results in constant intensity across the detector surface; non-zero offset results in a bull's eye pattern like that in figure 2.3 (which is what one would expect, since a flat mirror is a sphere with an infinite radius). In this case, we don't use right triangles. Instead, we use the fact that two interfering spherical wave-fronts will be tangent at the center of the detector, but due to their difference in radius, at the detector edge there will be a phase difference between the two waves. We set this difference equal to λ/4 and solve for maximum δz, similar to the previous analysis for offsets. Taylor series are used to simplify the analysis.
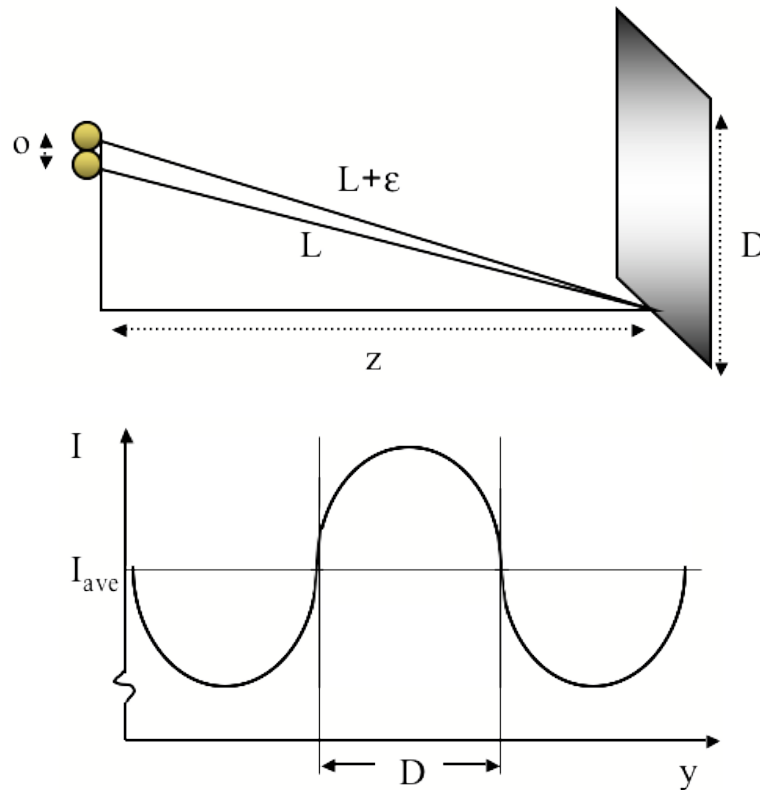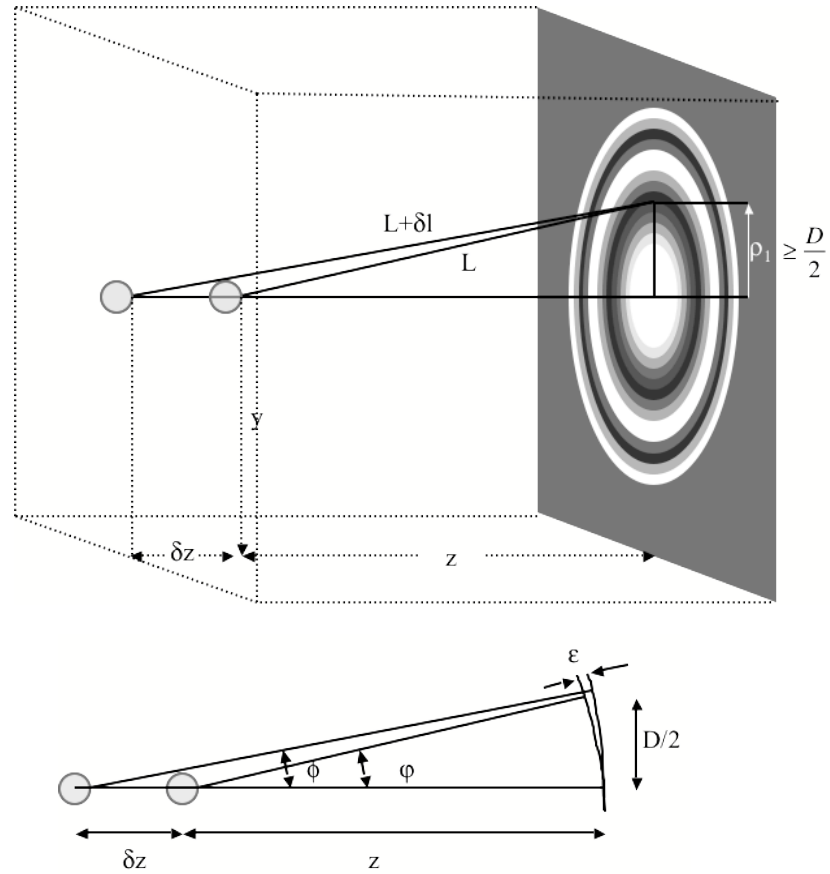
Figure 2.8: Finding the maximum δz in a two-sphere interferometer before more than one-half fringe is present on the detector of diameter D (i.e. set $\rho_1 = D$)*. The second figure shows the variables used to determine the maximum δz such that ε, the approximate phase difference at the detector edge, is equal to λ/4.

$$z \sin \varphi \simeq z\varphi = \frac{D}{2} \Rightarrow \varphi = \frac{D}{2z}$$

$$(z + \delta z) \sin \phi \simeq (z + \delta z)\phi = \frac{D}{2} \Rightarrow \phi = \frac{D}{2(z + \delta z)}$$

$$\varepsilon \simeq z(1 - \cos \varphi) - (z + \delta z)(1 - \cos \phi)$$

$$\cos \phi \simeq 1 - \frac{\phi^2}{2}; \cos \varphi \simeq 1 - \frac{\varphi^2}{2} \Rightarrow \varepsilon \simeq \frac{D^2}{8z} - \frac{D^2}{8z(1 + \delta z / z)}$$

$$\varepsilon \simeq \frac{D^2}{8z} - \frac{D^2}{8z}(1 - \delta z / z) = \frac{D^2 \delta z}{8z^2} = \frac{\lambda}{4}$$

$$\delta z = \frac{2\lambda z^2}{D^2}$$

---

* Detector diameter may be set to $2\rho_1$ as indicated previously; we use ρ_1 here to be conservative

Each use of the $\simeq$ symbol indicates use of a first order Taylor series approximation, which holds in this case because D << z, δz < z, λ <<< (δz, D, and z).

For z = 1m, λ = 1.5 µm, d=2cm, δz = **7.5 mm**; if z = 10m, δz = **0.75 m**.

Figure 2.9 shows results of a two-sphere interferometer demonstration.
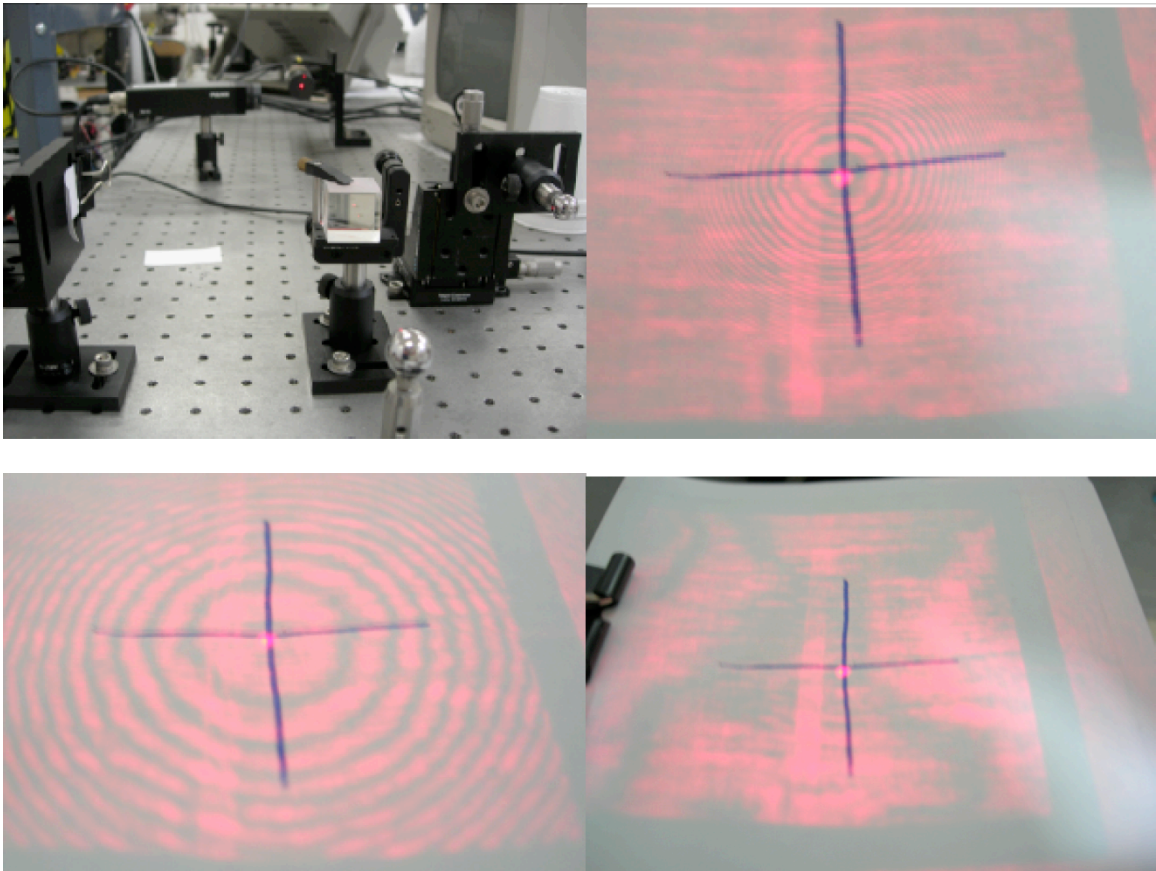
Figure 2.9: In the upper left, the sphere-sphere interferometer, with both spheres, beam splitter, Helium Neon laser, and viewing surface all visible with Z = 25 cm. The other three photos show the resulting interferograms when δz is reduced from 5 mm to 0. The "X" pattern in the last image is a result of imperfections in the two spheres— otherwise the 2 inch wide piece of paper would have complete interference across its surface. The central bright spot and vertical stripe in all of the images are ghost reflections from the beam splitter.

Visual inspection was used to determine the size/position of the central spot. As can be seen in fig. 2.9, a cross was drawn on a piece of paper and used to measure the

location of the rings. For z=25.4 cm, d=5 mm ("d" took the form of a circle drawn on a

piece of paper), and $\lambda = 0.63$ microns, δz was measured to be approximately 6 mm, and o

was measured to be approximately 50 μm. The values calculated with the equations are

$\delta z = 6$ mm and o = 15 μm (correct order of magnitude on both).

Now that some basic features of two sphere interference are understood, it is

possible to design an elementary feedback controlled compensator for the reference leg of

the interferometer, as shown in fig 2.10.
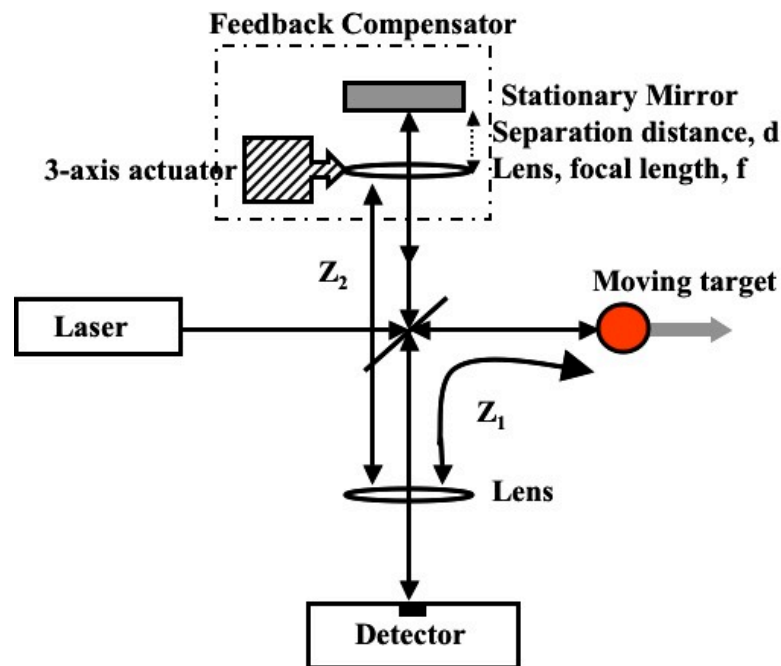
Figure 2.10: In this interferometer, the stationary mirror has been replaced with a compensator that matches the reference wave-front with the target wave-front for more complete interference, and greater signal, at the detector.

The feedback compensator is just a mechanism to produce light that has nearly

the same wave-front shape as the light reflected by the target—when the two waves

combine, interference signal intensity is optimized over a greater detector area than with

a simple iris.
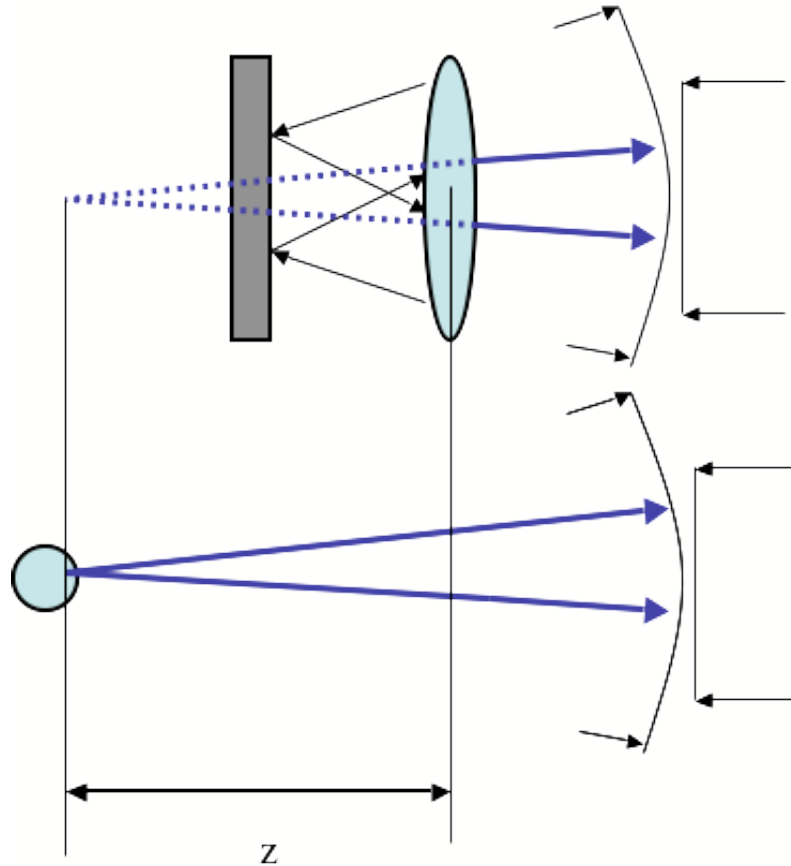
Figure 2.11: Here, it is illustrated how a lens/mirror combination can mimic a spherical reflector. A flat (laser) wave-front comes in from the right, is curved by a lens, reflects off a mirror, and is again curved by the lens before returning to the source.

It can be found, through repeated use of the lens/image equations, that the distance, d, from lens mid-plain (for a symmetric lens) to mirror surface is

$$d = \frac{2fz - f^2}{2f - 2z}$$

where f is lens focal length and z is the desired radius of wave-front curvature at the lens mid-plane; d < f for this equation to hold.

This equation is the basis for designing the lens-mirror system, and figure 2.12 shows how to select the lens. In that figure, d2 is the distance the lens must be translated

in order to create a change in z from 1 meter to 10 meters, d1 is the resolution required of the translator stage, and f is the focal length of the lens.

This chart demonstrates how wide the design space is for a simple lens-mirror feedback system—properties such as linear resolution, maximum displacement, and focal length can be optimized. Based on the chart, a 5cm focal length lens would require a translator with about 2 mm of travel, 1 micron resolution, and velocity capability around 2 cm/s in order to accommodate a target traveling from 1 m to 10 m at 100 m/s.
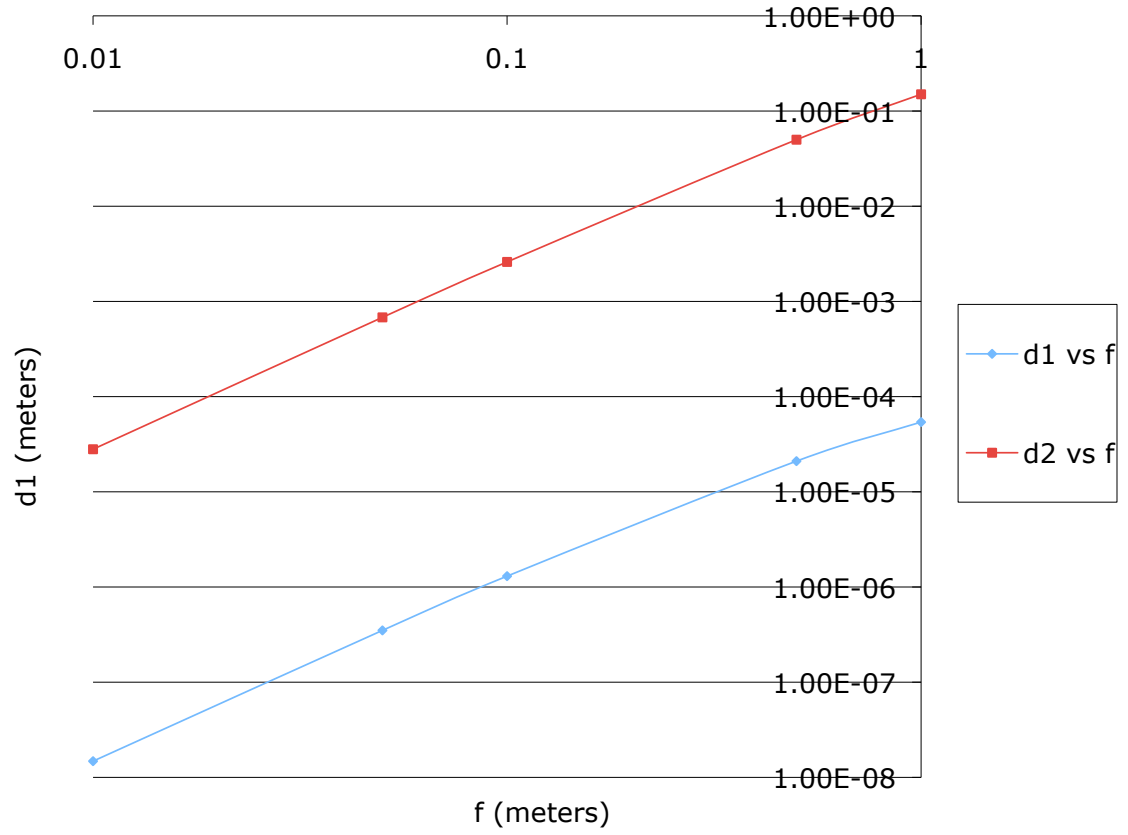
Figure 2.12: Guide to selecting lens focal length for lens/mirror feedback system. D1 is the net translation necessary to output a 1 to 10 m wavefront curvature; d2 is the required translator stage resolution to generate good interference at a 2 cm wide detector.

The resolution requirement is based on the spherical wave-front interference-matching criterion determined previously; i.e. with a 2 cm wide detector, one would want a maximum lens position error of 1 micron (in the z direction) to prevent the effective δz from becoming too great.

In the x and y directions, i.e. perpendicular to the light wave vector, the maximum wave-front offset (o) should be about 30 μm (again, based on the previous analysis of sphere-sphere interference, for z = 1 m). The lens must be moved as far as the target is expected to wander—up to 5 mm, with resolution better than 30 μm and speed up to 5 cm/s. The center of the wave-front corresponds to the center of the lens.

This analysis applies to scenario 1; in scenario 2, the system needs to make a single adjustment to match the wave-front expected from the target at glint. Since the Z robustness is quite high at such distances (δz ~ 75 cm) the lens would only need to move in the (x,y) axes.

The wave-front adapting mechanism can take target position information directly from the fringe counter and Poisson[*] spot measurements to adapt the wave-front in real-time. Alternatively, a wave-front measuring device can be added to the interferometer to get approximated data. One such system is called a "Shack Hartmann" sensor, where a lens array focuses light onto an array of position detectors; the variation in focus location for each lens is related to the wave-front curvature at the corresponding point in the beam. From the analysis earlier in this section, one can conclude that the wave-front

---

[*] The Poisson spot system has been demonstrated to meet precision requirements of IFE by Lane Carlson.

would need to be adapted at a rate above 10 kHz (likely 20 kHz); this rate depends on factors such as position and velocity of the target itself.

Ideally, this system does not introduce variable light path length into the interferometer, or reflections from the moving lens surface. Anti-reflection coatings would need to be as high-quality as possible.

There are alternatives to the lens/mirror system; in fact, the lens/mirror system may be useful more as an example than as a real design. For instance, one could replace the lens/mirror system with a high-tech deformable mirror, which could avoid all of the issues associated with a lens. Or, better yet, replace the lens with a liquid crystal spatial light modulator, or LC SLM (Shirai, Barnes and Haskell). The system used in (Shirai, Barnes and Haskell) was limited to around 1 kHz operation speed.

Yet another option is to replace the iris with an inexpensive liquid crystal display—and input a variable "bull's eye" pattern to block the undesirable half of the interference pattern. Perhaps even the element from a projector or computer monitor could perform this function. The bull's eye shape would be controlled by target position or wave-front sensing as described above. A modified computer monitor may even allow the direct use of Labview software to control the bull's eye pattern; one would need to remove all of the components that block the view through the LCD screen. The element from a projector may also fill this role quite simply, although projectors cost more than computer monitors. Either option allows one to simply plug a computer into a ready-built system. See http://www.youtube.com/watch?v=b7lWqKHpGuc&feature=related for a guide to disassembling a computer monitor for this purpose, or search Google for "LCD computer screen home made projector".

The LC SLM or standard LCD options appear to be simplest as they have no moving parts; the LCD and lens/mirror seem most cost-effective; and the deformable mirror is least attractive (most pricey, has moving parts). However, by far the simplest and most readily achievable option is the LCD computer monitor. This could be done for under $200 (assuming a computer with Labview is available to power it).

2.4. Electronic Filtering and Signal Amplification

It is desirable to have high performance signal filtering and amplification systems such that the output from this highly sensitive Michelson interferometer has a clearly defined signal. A signal to noise ratio on the order of 100 is desired such that the fringe counter has few extraneous counts (preferably none at all). So with this in mind, and the assumption that the real IFE system will have a weak signal that is buried in noise, we aim to design an electronic filter and amplifier that can cope with variable signal intensity (it falls off as $1/r^2$) and a variable signal frequency (the target is accelerated by gravity). For random/stochastic noise, amplitude decreases as $\sqrt{\text{Bandwidth}}$; so utilizing the narrowest bandwidth possible is advantageous. This is the concept behind a lock-in amplifier—extremely narrow effective bandwidth enables one to find extremely weak signals of interest from noisy, random background.

Our signal of interest has a very narrow bandwidth (essentially 0), so a narrow bandwidth electronic filter or lock-in amplifier would be ideal—except that the filter band needs to be adjusted as the target accelerates. In scenario 1, the frequency shifts by about 1 MHz as the target coasts 10 m to chamber center. In scenario 2, the frequency will change about 13 kHz during the 1 cm fringe count measurement. This is nearly negligible (i.e. target velocity is constant to 1/10000). But since the target velocity may

vary from shot to shot, the band-pass frequency will need to be determined in real-time; the band may be set to about 20 kHz to account for acceleration. Figure 2.13, a cartoon illustration, shows the expected signal from a fringe counter in the frequency domain. Note that most noise is in the lower frequencies for in-air applications. In the real power plant, this may vary significantly and depends on the chamber design.

Signal amplitude vs frequency
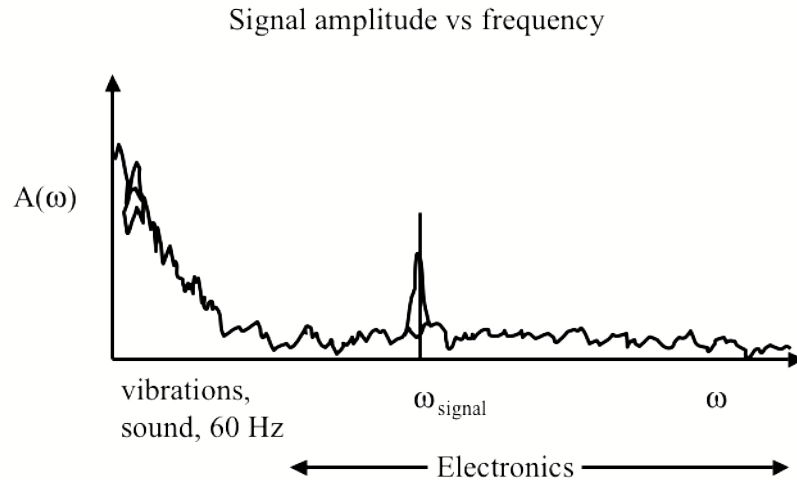
Figure 2.13: An example of the frequency spectrum output by the fringe counter. Mechanical/sound vibrations, 60 Hz electronic noise (from lights and amplifiers) dominates lower frequencies, while unavoidable electronic noise (dark current) dominates higher frequencies. The desired signal represents a very narrow spike, which shifts as a function of target velocity.

To set the filter band-pass as close to the signal frequency as possible, a real-time adaptive amplifier is indicated, as suggested in the scheme laid out figure 2.14. First a "broad" (actually as narrow as possible) band-pass filter limits the band to frequencies expected to contain fringe-count signal; this band may be determined by prior target velocity information. This may take the form of previous target injector performance or a pair of crossing sensors. Then resonators with closely spaced centers (and slightly overlapping edges) acts as a real-time Fourier transform. The resonator that has the

greatest amplitude response is selected and activates a resonant amplifier, resulting in the

final high-amplitude, low-noise signal.

An alternative to the 2nd stage in 2.14 is to use a pair of crossing sensors (as

indicated in the Demonstration section) at chamber entrance to measure target velocity;

the resonant amplifier is then activated directly from a target trajectory model.
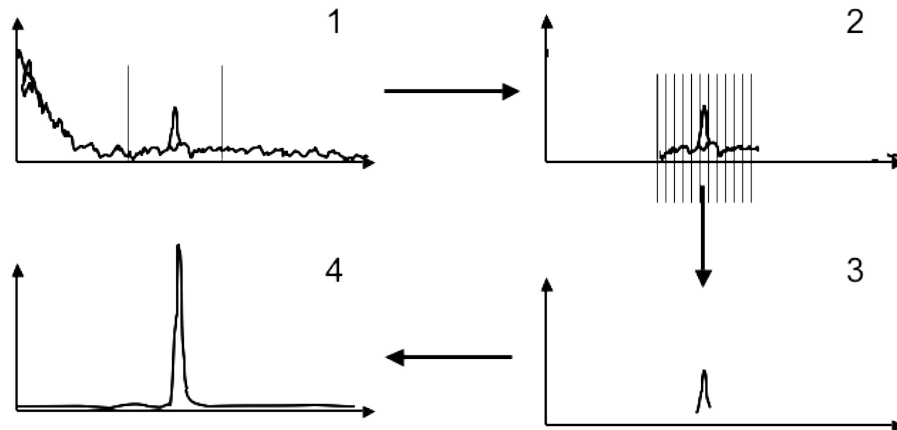
Figure 2.14: A four-stage signal conditioner amplifies the desired fringe-count signal in real time. Stage 1 is a high order (10th or >?) band-pass filter set to cover a range of expected frequencies. Stage 2 is a set of parallel resonators, in which the resonator with the highest amplitude signal selects a resonant amplifier.

To cope with the fact that the signal received from the target decreases as the

target moves away from the receiver, the electronics must be designed to cope with the

minimum expected signal. Then, perhaps the adaptive mechanism (LCD) could reduce

the signal intensity at close range to prevent overwhelming the photodiode, and allow full

intensity at greater target distances.

Since development of this system requires a close interaction between

constructing and testing precision electronics, as well as in-depth knowledge of the full-

scale injection process and capabilities (i.e. chamber gas or not, injector velocity

repeatability), a more detailed development has not been pursued.

2.5. Light Intensity Considerations

There are two competing factors with respect to fringe count laser intensity for IFE. First, the target is cryogenically frozen and will heat up if the fringe count laser is too intense and/or is incident on the target for too long. Second, the target reflects the equivalent of a point source of light back to the tracking detector, so that power received drops as $1/r^2$. These restrictions leave an upper and lower bound for selecting laser power. The lower value can be effectively decreased by more advanced amplification and filtering systems as outlined above; the ultimate limit would be the 20 or so photons per fringe suggested in (Petzoldt, Alexander and Carlson) with the use of a 200 mW laser.[*]

To avoid overheating the cryogenically frozen fuel during a 0.1 s injection period (10 m/ 100m/s), the target can't absorb more than about 0.1 W/cm^2 of laser power [conversation with Ron Petzoldt]. If the target is about 0.3 cm^2 in frontal area, and absorbs a (conservative) tenth of the incident radiation at 1.5 μm, the tracking beam is limited to about 3 W/cm^2 of laser power. Alternatively, in scenario 2 the 1 cm tracking period enables a 1000X increase in laser power (assuming no nonlinear heating effects). Actual target heating may vary, but scenario 1 limits the laser to a conservative 3 W/cm^2 that will serve as a baseline maximum for further analyses. With a 2 cm wide beam, and only half the light reaching the target, the laser could be up to 24 W if needed. Here we elaborate on the analyses of (Petzoldt, Alexander and Carlson) and (Flint) to provide a clear understanding of what determines the minimum laser intensity.

---

[*] This depends on ambient noise and the spectrum of that noise

Mirror

Beam splitter, 50%
transmission (optimum)

Laser, Power P

Target, Reflectivity R_t

Iris; $\rho = \sqrt{\lambda Z}$

Detector, noise $n*B^{0.5}$
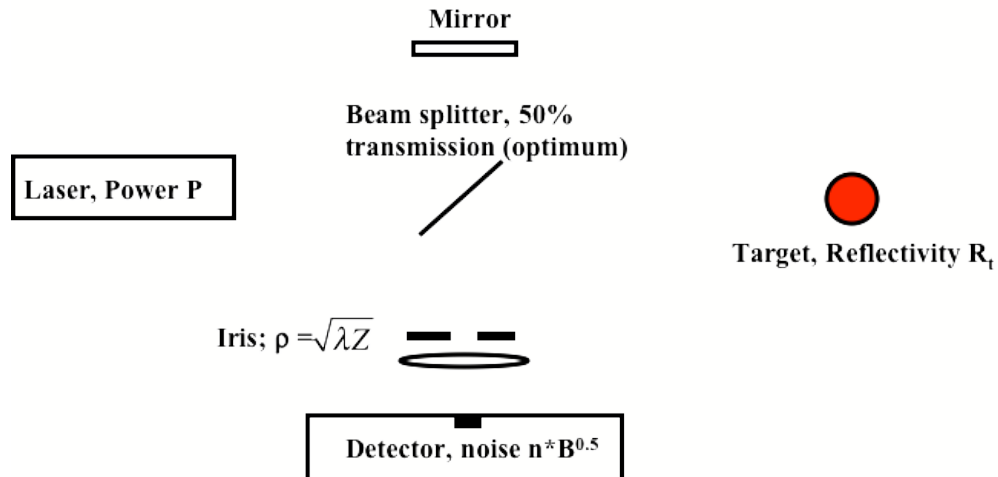
Figure 2.15: Geometry for calculating expected noise with use of an iris.

Defining some variables:

Z: target distance to receiver (iris or lens) (10 m)

A: Target radius (2 mm)

P: Laser power

E_1, E_2: Electric field magnitude at detector due to reference and target return waves,
respectively

P_1, P_2: Power magnitude at detector due to reference and target return waves, respectively

L: Laser beam radius

ρ: Receiver radius (iris) = $(\lambda Z)^{0.5}$

n [W/$\sqrt{Hz}$], Photodetector noise figure (from datasheet—divide dark current by detector gain),

B [Hz], Signal bandwidth (set by electronic filters post-detector),

$N = n \sqrt{B}$ [W], Noise from electronics, divided by detector gain to be directly compared with S,

S [W]: Power incident on photodetector

S/N: Signal to noise ratio

Assumptions:

-Beam profile is flat and circular in cross section

-Target velocity is a constant (100 m/s)

-Target position is maximum Z (10 m)

-Local Oscillator (reference beam) is equal in power to beam transmitted to target

-Noise is stochastic at frequencies of interest

First, the signal is proportional to the light intensity on the photodiode. From section 2.2, it was shown that intensity is proportional to the product of the two interfering waves' electric field magnitude (and power is intensity times area):

$$S_{amplitude} = E_1 E_2 \pi \rho^2 = \sqrt{I_1 I_2} \pi \rho^2$$

The intensity of the reference beam is then reduced by a factor of 4 upon reaching the detector due to passing the beam splitter twice:

$$I_1 = \frac{P}{4\pi L^2}$$

The intensity of the target beam return signal is evaluated based on geometric factors, as well as a factor of ¼ due to the beam splitter:

$$I_2 = \frac{P}{4} \frac{A^2}{L^2} \frac{R_t}{4\pi Z^2}$$

Incorporating these into the signal equation results in:

$$S = \pi \rho^2 \sqrt{\frac{P}{4\pi L^2} \frac{P}{4} \frac{A^2}{L^2} \frac{R_t}{4\pi Z^2}} = \pi \rho^2 \sqrt{\frac{P^2}{16} \frac{R_t}{16\pi^2 Z^2} \frac{A^2}{L^4}} = \frac{P}{8} \frac{A}{L^2} \frac{\rho^2}{Z} \sqrt{R_t}$$

which can be further reduced by substituting $\rho = \sqrt{\lambda Z}$, and dividing by $N = n\sqrt{B}$ to get S/N:

$$\frac{S}{N} = \frac{P}{8}\frac{A}{L^2}\frac{\sqrt{\lambda Z}^2}{Z}\frac{\sqrt{R_t}}{n\sqrt{B}} = \frac{P}{8}\frac{A}{L^2}\frac{\lambda}{n}\sqrt{\frac{R_t}{B}} \ ^*$$

Now we introduce 2 λ/4 plates and a polarizing beam splitter into the interferometer, as well as eliminating the iris through use of a dynamic LCD bull's eye. Then the receiver can have the same radius as the laser beam, but only receives half of the incoming light.
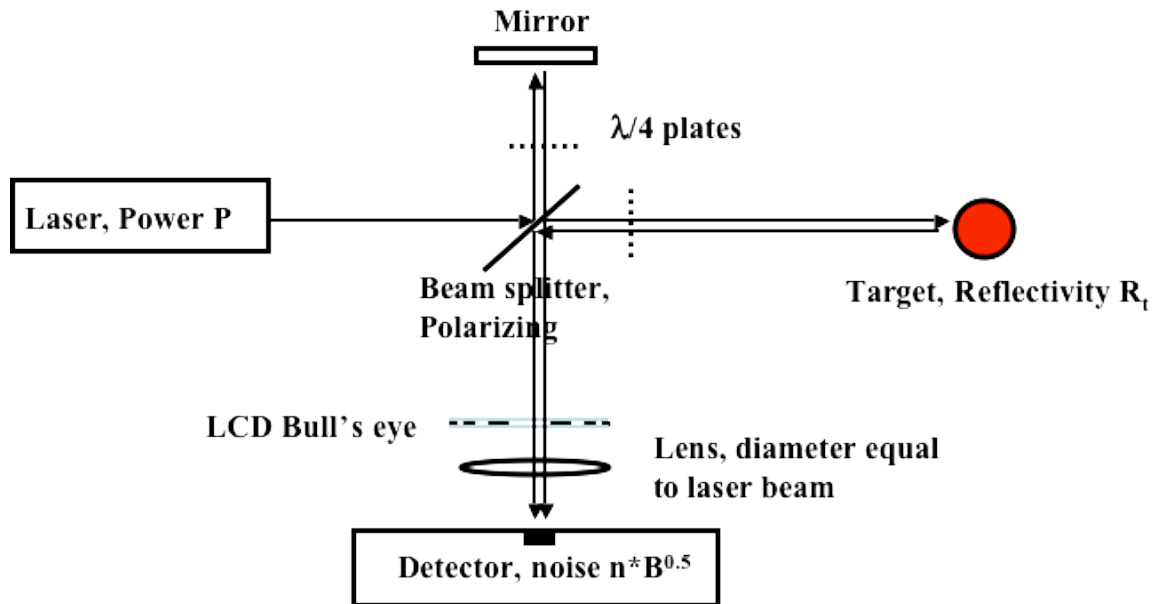
Figure 2.16: Eliminated iris (with LCD) and use two quarter wave plates. Laser is unpolarized; effect of polarizing optics is to double received light intensity in comparison with an ordinary beam splitter.

The result is a factor of 2 increase in S/N as well as replacement of ρ with L:

$$\frac{S}{N} = \frac{P}{4}\frac{A}{L^2}\frac{L^2}{Z}\frac{\sqrt{R_t}}{n\sqrt{B}} = \frac{P}{4}\frac{A}{nZ}\sqrt{\frac{R_t}{B}} \ .$$

We can substitute some realistic values to illustrate the difference. For Z = 10 m, n = 2.5 pW/ , A = 2 mm, λ=1.54E-6 m, L = 1 cm, B = 1 MHz, Rt = 1, with the first setup;

$$S / N = 1540P$$

---

and with the second setup, we get a factor of 13 improvement:

$$S/N = 20000P \ .$$

To check this analysis, we'll plug in some values from the demonstration (which used the first setup):

$Z = 0.3$ m, $n = 15$ pW/$\sqrt{Hz}$ [*], $A = 2$ mm, $\lambda = 1.54$E-6 m, $L \sim 4$ mm, $B \sim 1$ MHz, Rt = 1, P = 0.06 W;

$$S/N = 770P = 46.2 \quad .$$

From observations, this is close—compare with the upper trace in figure 2.18. The value of L is an approximation, since the beam was roughly Gaussian with a 1/e2 radius of 8 mm. The bandwidth is poorly defined since 2 sets of low order filters were in use—1 MHz is a conservative value; the true value is closer to 500 kHz.

From experience, it may is desirable to get the theoretical S/N as high as 103 to ensure countable signal and overcome any unknowns. By the first analysis, a laser of power 1 W is the minimum to attain a S/N of 103. By the second analysis, a power of 0.1 W is needed. However, at such laser intensities, the photodiode will be saturated if the reference leg of the interferometer receives equal power as the target leg.[†] Therefore, it will be necessary to offset the two power levels to prevent damage to a sensitive photodiode; this in turn will require higher laser intensity.

---

[*] The noise was calculated as 2.5 nW/√Hz for the detector and 12 nW/√Hz for the AM 502 differential amplifier, as designated on page 2-2 of the AM 502 Instruction Manual; the value was originally quoted as V/√Hz, but one can divide this by the net system gain (~50000) to get the equivalent in W/√Hz at the photodiode.
[†] Actually, for the 10 m configuration, any laser power over ~200 mW will saturate the detector.
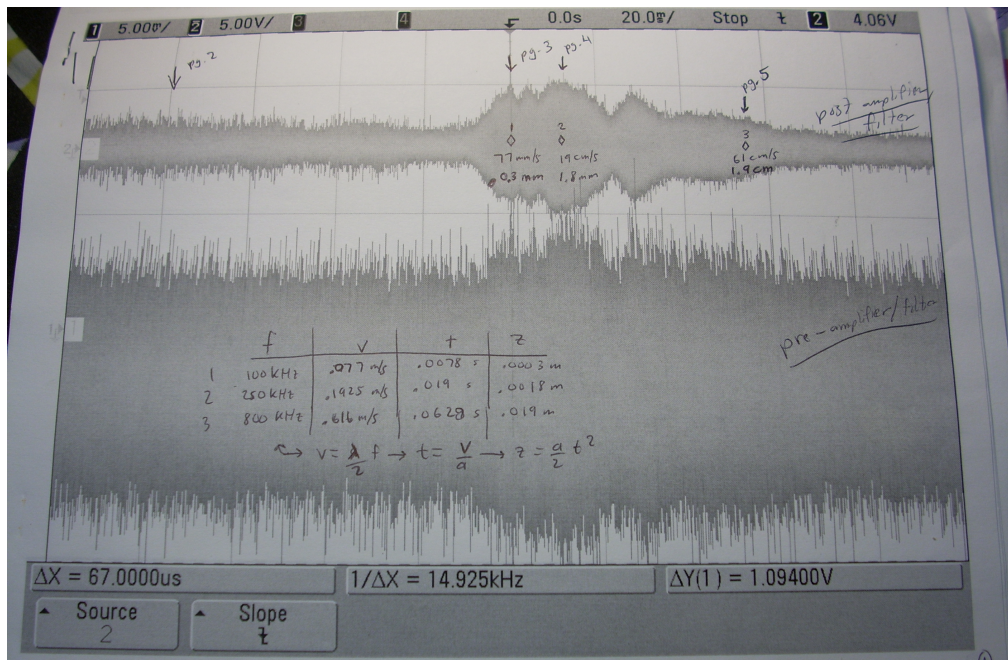
Figure 2.17: Demonstration signal results. Top signal was filtered while bottom has not. Data was visible from oscilloscope trigger point (t = 0.0 s) to about t = 56 ms; signal is caused by target starting from V=0 under gravitational accelerarion. At 56 ms velocity is 0.6 m/s and distance is 2 cm. This trace motivated the upgrade to the verifiable real-time demonstration presented in section 3.
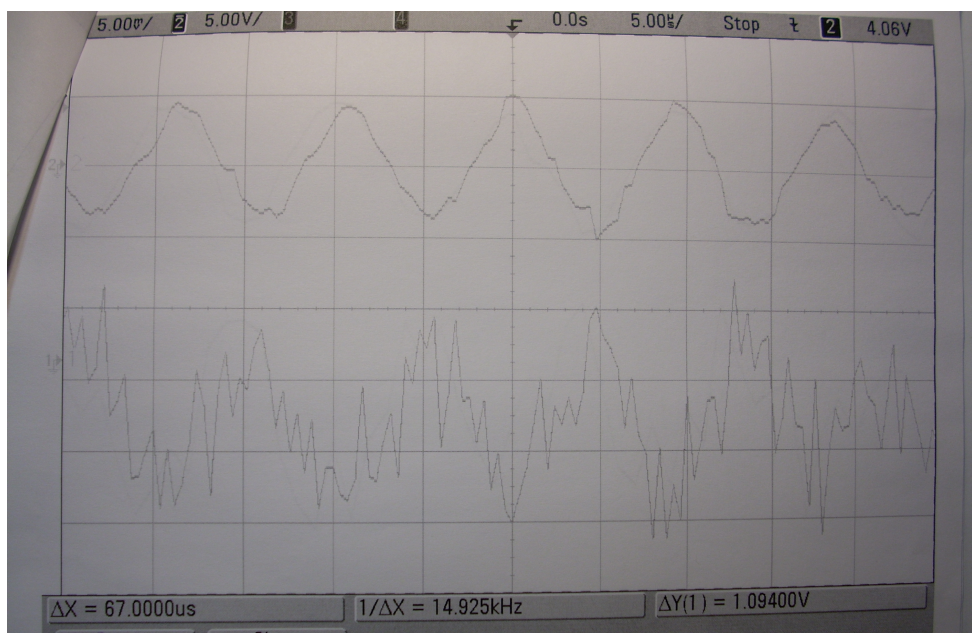
Figure 2.18: Demonstration signal results. The top signal has been filtered while the bottom has not (the amplifier/filter inverted the signal). This is the same as the trace in figure 2.17, but with a much finer temporal scale. S/N is approximately 3 in the lower trace, and perhaps 10-20 in the upper trace.

Suppose the maximum total power at the photodiode is limited to 10 mW (half the maximum for the photodiode used in the Demonstration). Since the power of the light returning from the target is negligible, this places a 10 mW restriction on the light returning from the reference leg of the interferometer. The simplest case is the first one considered previously, with no polarizing optics and an iris. Then the reference arm of the interferometer will need an intensity-reducing filter, as shown in figure 2.19. The following analysis incorporates this fact to determine S/N.

First, one needs to evaluate the total power incident on the photodiode due to the reference beam (written as $P_{d\text{-}r}$) to determine the reduction factor F:

$$P_{d\text{-}r} = \frac{\pi \rho^2 F^2 P}{4\pi L^2} = \frac{\lambda Z F^2 P}{4L^2} \Rightarrow F = 2L\sqrt{\frac{P_{d\text{-}r}}{\lambda Z P}}$$

Then S/N is evaluated as follows:

$$S\!/\!N = \frac{1}{n\sqrt{B}}\sqrt{P_{d\text{-}r}\frac{P}{4}\frac{A^2}{L^2}\frac{\pi\rho^2 R_t}{4\pi Z^2}} = \frac{A}{4L^2 n}\sqrt{\frac{\lambda Z F^2 P}{4L^2}\frac{P}{B}\frac{R_t\lambda}{Z}} = \frac{\lambda FAP}{8L^3 n}\sqrt{\frac{R_t}{B}} = \frac{A}{4L}\frac{1}{n}\sqrt{P_{d\text{-}r}\frac{P}{B}\frac{\lambda R_t}{Z}}$$

For Z = 10 m, n = 2.5 pW/ , A = 2 mm, λ=1.54E-6 m, L = 1 cm, B = 1 MHz, Rt = 1, P = 1 W and P$_{d\text{-}r}$ = 0.01 W;

$$F = 2L\sqrt{\frac{P_{d\text{-}r}}{\lambda Z P}} = 0.5$$

$$S\!/\!N = \frac{A}{4Ln}\sqrt{P_{d\text{-}r}\frac{P}{B}\frac{R_t\lambda}{Z}} = 785$$

which is just about the desired signal level. If instead the LCD and polarization optics method is pursued, the power required would be reduced. Note that these revised relations are only necessary if P$_{d\text{-}r}$ exceeds the detector limit.
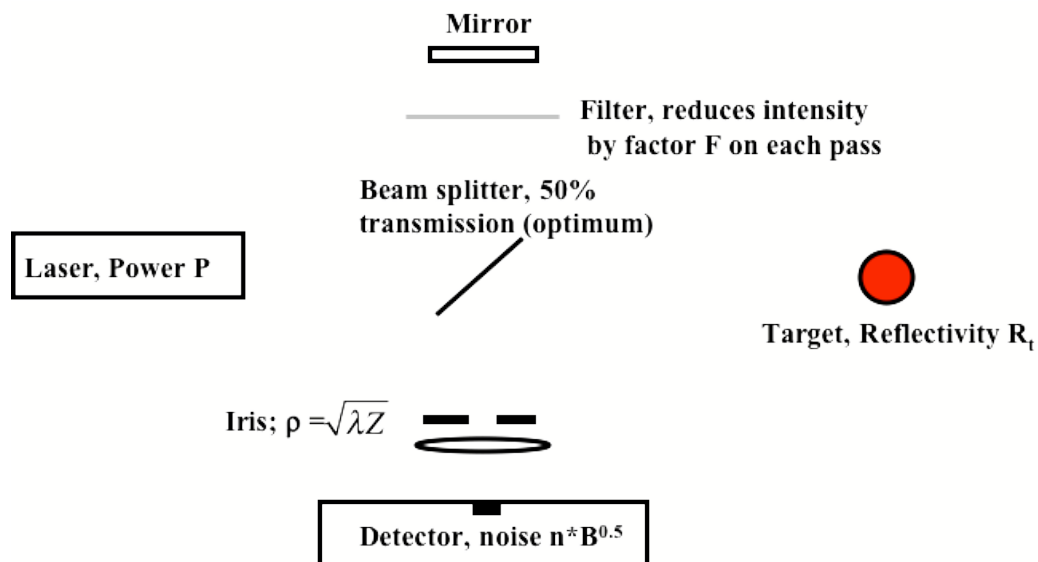
Figure 2.19: Introducing a filter to prevent saturation of the detector.

2.6 Receiver Design

"Receiver" may be defined herein as those components that convert the interference pattern into an electric current; in figure 2.16, this would include the lens, iris, and photodiode (but not the amplifier attached to the photodiode).

The goal is to use a photodiode that can handle the expected ≤133 MHz fringe count signal while maintaining low noise (~pW/$\sqrt{Hz}$), high sensitivity, and also the ability to handle moderate power levels (~10 mW). This indicates a detector of up to 1 GHz bandwidth, since response tends to taper off as the signal of interest nears the maximum. The easiest option is a solid-state InGaAs photodiode—similar to the one used in the demonstration, which was 100 μm diameter, damage threshold of 20 mW and bandwidth of 10 MHz (New Focus 2117). The New Focus 1617 can handle up to 800 MHz, but has a low 2 mW damage threshold and 20 pW/$\sqrt{Hz}$ of noise. These are tolerable values—but as shown in the previous section, the 10X lower damage threshold and 10X higher noise will dramatically increase the needed laser intensity. Detector

selection is an important factor, with the common theme that smaller detectors are usually

faster—so it is important to put optics in front of the detector that can properly focus as

much light as possible onto the diode surface.[*]

From "Melles Griot: The Practical Application of Light," which is an optics guide

accompany to Melles Griot's optics catalogue, the following three factors determine

minimum focal spot size for a given lens/aperture combination:

Minimum Gaussian beam waist diameter for a given lens focal length and beam

diameter:

$$d = (\frac{4\lambda}{\pi})(\frac{f}{D})$$

Minimum spot size due to spherical aberration (imperfect lens) is:

$$d = \frac{.067f}{(\frac{f}{D})^3}$$

Minimum spot size due to diffraction (Airy disk diameter) is:

$$d = \frac{2.44\lambda f}{D}$$

To optimize the lens/detector combination, the minimum spot sizes must be at least a

factor of 2 smaller than the diameter of the photodiode so that all light is collected. Either

the Airy disk diameter or spherical aberration dominates; then the lens focal length can be

---

[*] Upon this writing, a method for increasing receiving power was conceived: optically amplify the signal incoming from the target. An amplifier could potentially amplify both outgoing and incoming signals. (Pierrottet, D. 2005) demonstrates amplification of the outgoing signal (via a Fiber Amplifier); in figure 6 of that reference, the "receive" leg of the setup, which is a plain fiber coupled to the photoreceiver, would incorporate a fiber amplifier that can accommodate a range of wavelengths. The author is unaware if this is physically possible. Perhaps a Zeeman laser cavity could be used to amplify such a light signal—the B field would be adjusted until maximum amplification is achieved to match the signal frequency.

selected based on the beam diameter, D; maximum spot size, d; and lens focal length, f. Unless aspherical lenses are used, spherical aberration determines the minimum focal length, while diffraction determines maximum.

2.7. Error Sources

This section is designed to systematically investigate all the sources of error in a fringe counting system. Table 2.20 below summarizes the text of this section, in the same order.

The count vs. time precision is limited by the time base of the counter (~1/speed). So, for the 133 MHz full-scale fringe counter, at least a 500 MHz counter is desirable. For example, there would be a 0.2 fringe variability in the timing of each count, leading to a $\lambda/10$ error ($0.2*\lambda/2$ μm/count) but this error is not cumulative, as each fringe is counted uniquely. So the net error from the counter time base is about 0.15 μm, a negligible number.

Lateral motion of the target will introduce some count error. The error depends on the extent of target wander, the design of the interferometer (i.e. if wave front correction is used or not), as well as target-to-detector distance. For a simple iris receiver, maximum expected error is ~2 counts, or a maximum error of λ, assuming that the iris is set to ρ_1. Any motion beyond ~ρ_1 results in reduced signal and loss of counting ability, so the system would become ineffective beyond. Wave front control or an LCD bull's eye would prevent this error, while adding robustness to the system.

Laser intensity fluctuations are a potential source of error. In addition to using a stable laser, it may be necessary to use signal normalization to account for intensity fluctuations from the laser as well as fluctuations in power returned from the target

(which decline as $1/Z^2$). The signal would be electronically divided by the un-interfered

signals (both independently); analog circuits can be used to perform division. (Barker and

Hollenback, Laser Interferometer for Measuring High Velocities of any Reflecting

Surface) One may also use a heterodyne interferometer to reduce this issue (see

introduction). Signal subtraction was pursued experimentally without success (see figure

2.21 below) and has since been abandoned.

Error Source	Type	Error	Reducible?
Counter	Random	1/MHz s	negligible
Lateral motion	Random +	e < 1.5 μm	Yes
Laser intensity	Random +	0 < e < ?	Must
Laser wavelength	Systematic or Random	0 < e < ?	Must
Target radius	Systematic or Random	? < e < ?	Yes*
Target Out-of-round	Random +	0 < e < 40 μm	Yes^
Crossing Sensor	Random	3 < e < 10 μm	Maybe
Interferometer vibration	Random +	??	Must
Start/Stop count	Random	e < 1.5 μm Total (rms) 4 < e < 10 μm	Yes
*May be reduced by measurement in-situ ^May be reduced by spin--see text			

Figure 2.20: Sources of Error

It is important to stabilize laser wavelength, since it is the ruler against which

fringe counting measures distance. For scenario one, wavelength must be constant to 1

part in 10^6 (e.g., 1 pm for 1 μm light). A Fabry-Perot cavity can enable 1 in 10^5 stability,

however 10 times that is needed. This may require the use of a precision wave-meter to

measure and feedback wavelength to calibrate measurements in real-time. Hovemere,

Ltd., builds wavelength measurement systems with 5 fm measurement precision (at a cost, of course). Either way, the wavelength stability requirements are readily achievable. Commercially available diode lasers can meet the stability requirements, as does the laser used in the demonstration here; by thermally stabilizing a diode laser, one can control the resonator cavity size and resulting laser frequency, the same as for a gas laser.

For the second scenario, in order to predict the position to 10 μm after 10 cm of travel, the velocity needs to be known to approximately one part in 10^4, or 1 cm/s for V=100 m/s. This assumes the glint and velocity measurements are performed 10 cm before chamber center. Again, this is readily achievable in practice.

The author is unaware of previous target radius requirements that indicate the level of consistency from the target production process. Therefore, it is assumed here that some system needs to measure target radius in-situ before injection, such that the fringe counter can be calibrated. The error in this measurement then needs to be included in the RMS fringe count error presented in table 2.20.

In a worst-case scenario, the target may be up to 1% out of round. Then the reflection point of the fringe counter beam may oscillate by as much as 40 μm, introducing a position error (where position is defined relative to center of mass) at a given point in time. A spinning target will average out the effect. The maximum spin rate is a function of target velocity; above a spin rate of 2.5 MHz, extra fringe counts will be generated as the bump (figure 2.22) reverses the apparent target velocity (100 m/s ÷ 40 μm = 2.5 MHz). However, the target is more realistically limited by material strength to kHz spin rates.
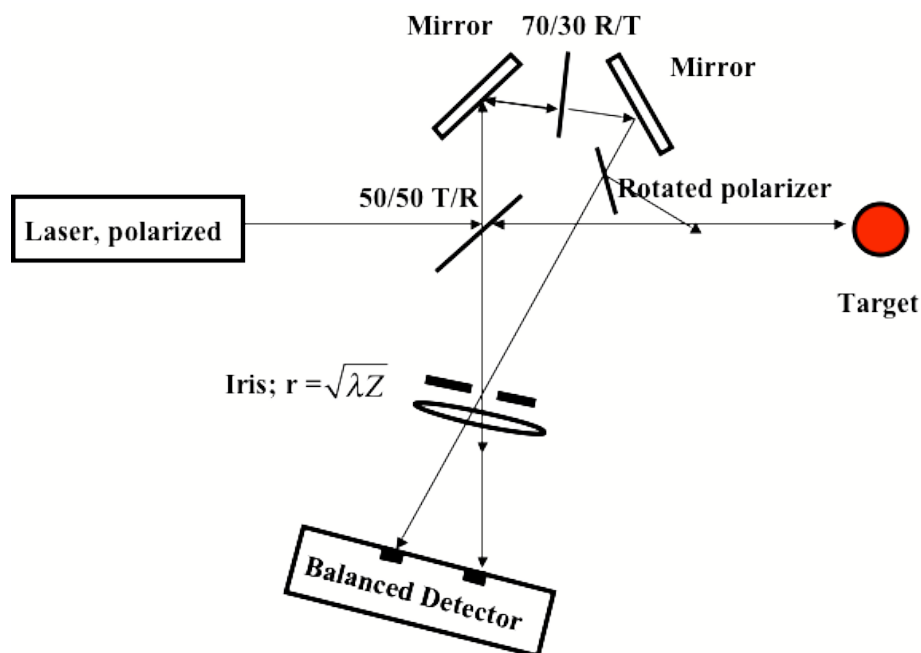
Figure 2.21. Experimental attempt at signal subtraction. Properly aligning the two beams was a serious difficulty, as both beams need to be focused identically by the lens. Also, the iris needs to sample the same portion of the beam due to its Gaussian distribution. Ultimately more, not less, noise was apparent in the signal. Note that no isolator is present; also the main beam splitter was a pellicle, chosen for its lack of dual reflections (but it introduced vibrational noise). The rotated polarizer was a high extinction ratio Glan cube mounted in a precision rotator. This scheme could be replaced with signal normalization instead of subtraction by constructing custom detector electronics.
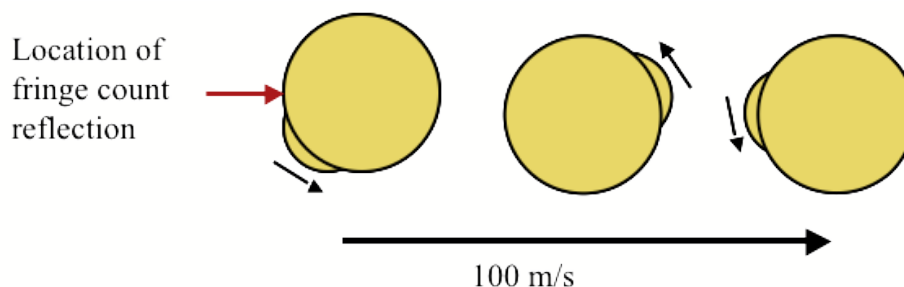
Figure 2.22: Spinning out-of-round target modeled as a perfect sphere with a rounded protrusion of 40 μm height.

The minimum spin rate for fringe counting depends on what scenario is

considered. For scenario 1, the target needs to spin rapidly enough that oscillations in

target velocity can be attributed to spin, rather than another cause. This, therefore, requires a real-time FFT on the data to find the oscillation frequency and subtract it from the data. To find the frequency with perhaps 1% accuracy would require about 100 cycles during the 0.1 s coasting phase of injection—which then requires a spin rate of 1 kHz (of course, a 10% accuracy may be acceptable as well—leading to a minimum spin rate of 100 Hz). For scenario 2, the target can have 0 rotation since only velocity matters, not position. In fact, 0 spin would be preferable here since all that is desired is a velocity measurement with 1 cm/s accuracy from a 1 cm, 0.1 ms interval. If the target spins faster than 250 Hz, the 40 μm bump will generate over 1 cm/s apparent velocity—but this error will not be detected since less than one full rotation will be completed in that time frame. Under 250 Hz (or ~100 Hz) does not significantly impact the velocity measurement. So ~200 Hz is a good upper limit. On the other hand, if the target is spinning fast enough, the velocity fluctuations will average out. If the spin rate is 10n kHz (n is an integer; n rotations per 0.1 ms interval = 10n kHz), the average velocity will be accurate over the 0.1 ms interval. So to conclude this analysis, scenario 1 requires a spin rate ~1 kHz; scenario 2 requires a spin rate either < 200 Hz or 10n kHz (where n is an integer).

Vibrations between components within the interferometer can introduce a random, positive error. It may be possible to eliminate all open space between components, thereby reducing the effects of vibrations, as well as secondary reflections. This may come in the form of either optical fiber connections between components, or bonding components to optical substrate (i.e. all components permanently embedded in glass). See figure 2.23 below.
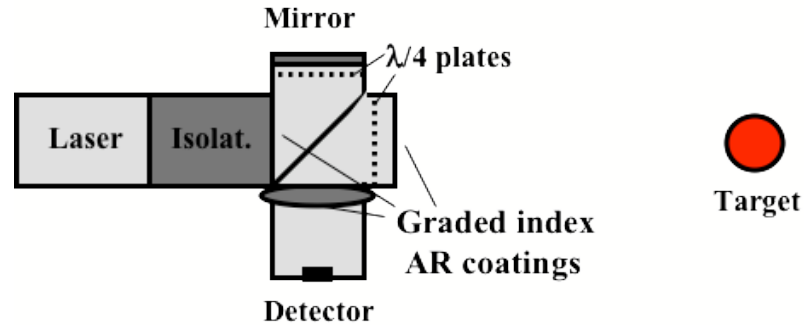
Figure 2.23: A cartoon example of a no-free-space interferometer for fringe count detection. Wavefront correction systems/iris are not shown but could be incorporated. Graded index coatings are used at free surfaces and joints between differing index of refraction materials to prevent superfluous reflections. The whole thing would be thermally and vibrationally stabilized.

The limited resolution of the fringe counter introduces up to ±2 erroneous counts (net error of ±λ). The resolution can be improved by using several threshold levels per fringe, i.e. more than one count per fringe. If it is decided at some point to use either a longer wavelength of light, or a frequency-reducing heterodyne system, this can be used to improve resolution.

3. DEMONSTRATION

(Spalding, Tillack and Carlson) presents an oscilloscope trace resulting from dropping a target and collecting the signal reflected from it. That demonstration was limited in that it was not possible to quickly and repeatedly track the target to the desired precision and accuracy, as is desired for a power plant (although, the information contained in that trace is still valid—i.e. the tracking system worked). The demonstration also lacked any sort of direct comparison of measurement accuracy (even though the interferometric data is probably more accurate than any other measurement data). These inadequacies in the previous experiment were ideally remedied with the demonstration presented here. Two crossing sensors, with separation distance stable to ~5 μm, were used to trigger the start and subsequent stop of counting fringes. A simple, precise, and fast[*] target release mechanism replaced the previous vacuum-based system. A custom fringe counter and trigger were constructed to operate in real time. Each system is presented in further detail, along with appropriate figures and schematics, in sections 3.1 to 3.3; then results from this demonstration are presented in section 3.4.

3.1. Setup: Electromagnetic Target Dropper

Figure 3.1 shows a schematic of the target dropper. 4 1.5-volt (AA) batteries in series supply voltage to a simple circuit, where the output current is adjustable and reversible via a potentiometer and switch. The current is sent through an electromagnet, made by wrapping solenoid windings on a pin (removed from a thumb tack).

To operate: maximize current setting and place a steel bb at the tip of the pin. Wait until the bb stops oscillating, and then minimize the current. When ready, reverse

---

[*] ~30 seconds total time from placing target on mechanism by hand, to dropping target.

the current direction to instantaneously release the sphere. If the current is not reduced

before reversal, the target will not be released; instead, the magnetic field induces a

reversal of the magnetization of the sphere and the target stays put. This procedure

requires less than a minute to perform, and performs very reliably. In a test performed in

an enclosed PVC tube at atmospheric conditions, drops consistently fell within a 1mm

diameter circle after falling over 1m from the electromagnet, (fig. 3.2) where stochastic

("knuckle ball") drag effects generate unavoidable lateral target motion (R. W. Petzoldt).
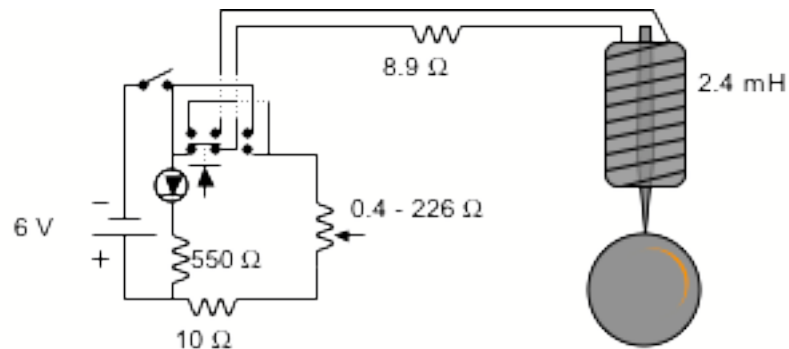
Fig. 3.1. Schematic of the custom electromagnetic target dropper. A circuit
outputs an adjustable and reversible current that activates a 2.4mH electromagnet. The
force on the 4mm steel sphere is symmetrical with respect to gravity.

The force on the steel ball is related by the following derivation:

$$F \propto \frac{mB_t}{R}$$

$$B_t \equiv B \text{ inside target}$$

$$m \equiv \text{moment induced in sphere}$$

$$B_t \propto B_i / (rR)$$

$$B_i = B \text{ inside thumb tack} \propto iN$$

$$i = current, N = \text{windings/length}$$

$$r = \text{radius of thumbtack}$$

$$F_{magnetic} \sim \nabla(m \bullet B_t) \sim \frac{mB_t}{R}$$

The magnetic force on the sphere is proportional to both m, the moment induced

in the sphere, and B_t; both of these are proportional to B_i. But it is known that the sphere

will experience hysteresis—that is that m will remain at some level even after B_i is removed; also, B_i will remain nonzero even when i is zero.
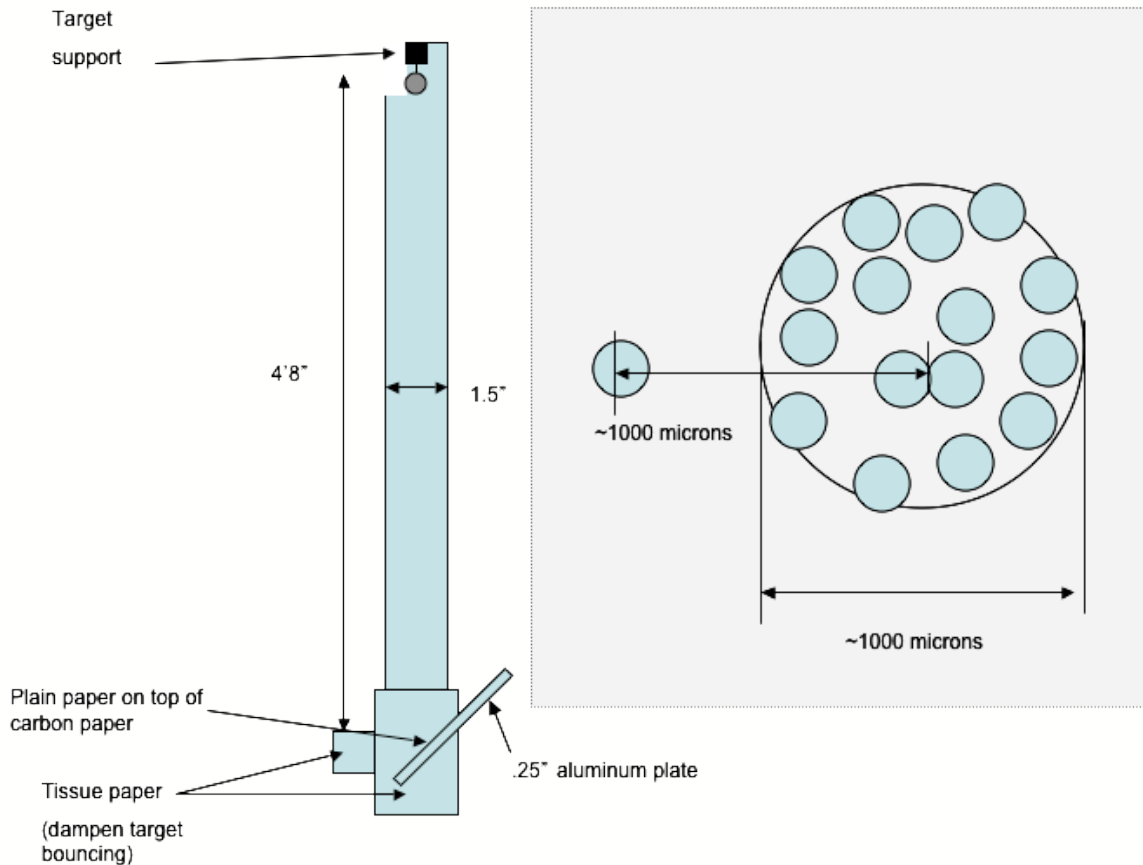
Figure 3.2. Schematic of a test to demonstrate performance of target dropper (not to scale). An ~5 foot tall, 1.5 inch inner diameter PVC tube was sealed at one end, and the target dropper was attached at the other. A slot was cut at the base, allowing insertion of a 0.25" thick aluminum plate with plain paper taped on top of carbon paper. After releasing about 15 targets in this configuration, the spread of resulting dots was about 1mm as shown at right; one drop was an outlier. Previous analyses at General Atomics had shown that nonlinear drag would cause such targets to wander about 0.5 mm in air under similar circumstances, so this performance is consistent with that analysis; the target dropper is not introducing a significant lateral motion to the targets as they are released. Therefore, there is expected to be very little lateral motion during the 1.5 cm drops performed in the demo.

Therefore to make the force either 0 or repulsive, the current must be reversed, but to a small enough degree that m is not reversed; then the force will be repulsive for a short

time period (before m is reversed). If the current is too high upon reversal, m is simply reversed and the force holding the target in place is not reversed, and the target isn't released.

3.2. Setup: Crossing Sensor and Triggers

Fringe count measurements needed to be validated against some other measurement to ensure that the information has meaning. A mechanism was desired that could verify a sub-10-µm measurement accuracy and precision. The following system seems to meet this criterion while also being relatively simple to assemble. Two crossing sensors, of known separation distance, are used to trigger the start and stop of fringe counts that result from the motion of a falling metal sphere.
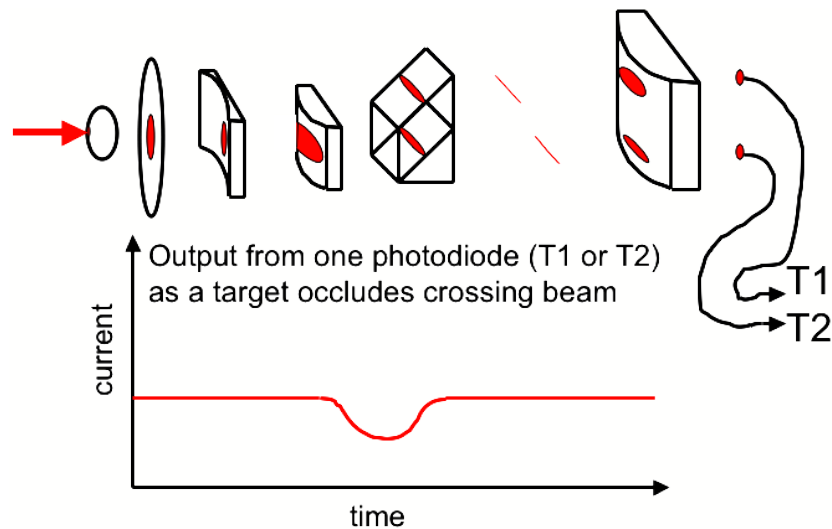
Figure 3.3: Crossing sensor setup. A helium neon laser beam is sent through a series of optics to generate two flat beams. The angled red lines in the figure represent the focal lines of the two beams, and the rightmost components represent two photodiodes with wires coming out. Photodiodes are a standard PIN Photodiode, 0.86 X 0.86 mm square; 2 ns response time;10 µA response at 1 mW flux; ~1 nA at 0 flux.
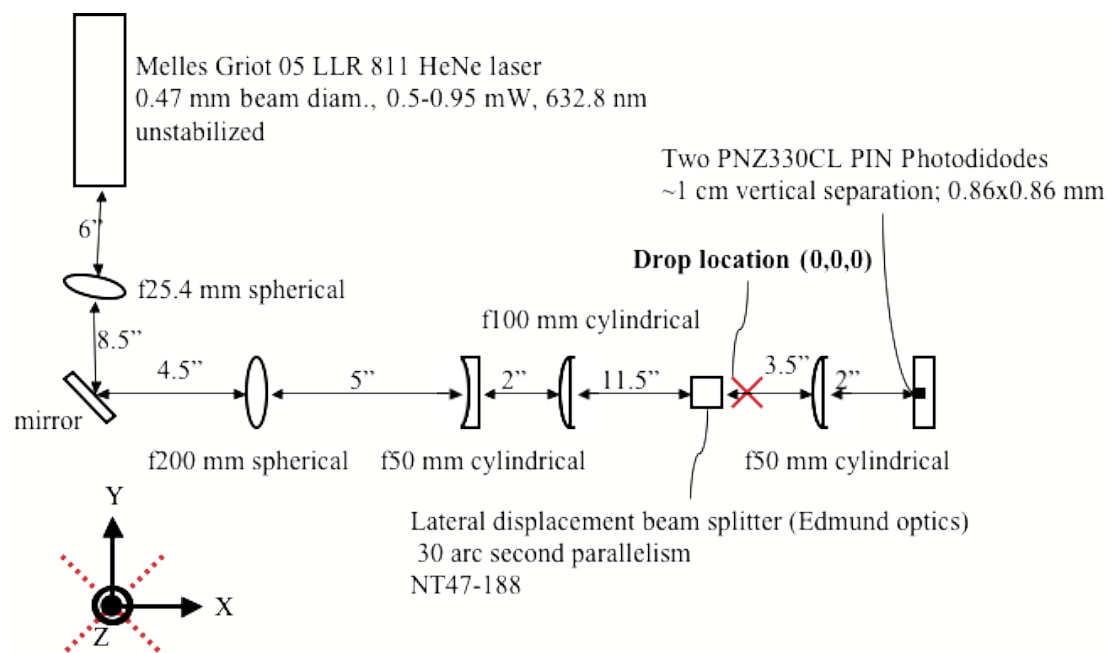
Figure 3.4: Full crossing sensor layout, not to scale. Coordinate axes are labeled; origin is at table level and target drop point. Note that the laser is NOT stabilized; ideally it would be. The plane (0,Y,Z) corresponds closely to the focal lines of the two beams. The focal lines had thickness around 100 μm.

Figures 3.3 and 3.4 show the optical system that generates two flat beams that have a separation distance stable to approximately 5 μm. The two beams are fiducials whose separation distance is then measured and compared with the fringe count measurement. The beams are generated from a single Helium Neon laser with 470 μm beam diameter. This beam is passed through a short focal length lens in order to generate a large beam divergence. Then the diverging beam passes through a long focal length lens, positioned to focus the light at about 0.3 m away.

Then, a pair of cylindrical lenses is used to collimate the light in one-dimension, while the other dimension continues to a focus; this generates a nice flat beam, with thickness of approximately 100 μm (measured by translating a pinhole across the beam). Also, if the lenses are arranged properly, this focal point will not wander vertically even if the laser output itself wanders. Ideal lenses take all parallel incoming light and focus it

to a single location, so that in this case, if the light from the laser is wandering but remains parallel, it will still focus to a spot that is well located in space and time. This was roughly verified by slightly nudging the laser up and down, while observing the location of the focal point.

The next to last optical component is a parallel output beamsplitter (the two beams are parallel to within 30 arcseconds) with a 1 cm output separation. The separation adds 1 cm of path length to the upper beam, thereby moving the focal point of the beam backwards a cm. Due to reasonably good performance as-is, a beam splitter without an offset was not pursued[*].

To measure the distance between the two beams, a small pinhole was translated using a calibrated translator, until the output of the photodiode was a maximum. Therefore the "beam center" is the point of peak intensity within the beam. The limit to this method was simply ability to resolve minute variations in beam intensity via observing the signal level with an oscilloscope, as well as the 2.5 μm resolution of the translator stage.

The measurements showed a beam separation that varied over time at a given location, and from point to point, by at most 10 μm (neglecting outliers at the edges of the beam, beyond where the target would be expected to fall). Higher error was found further away from the center and further away from the focal plane in general. Each crossing sensor light signal is converted to current via a photodiode[†]. The photodiode current from both photodiodes is then fed into a single analyzing circuit, which first

---

[*] Use mirrors to equalize light path lengths.
[†] The signal on the photodiodes was maximized and nearly equal (perhaps a 1% difference), although the derivative is what matters, not the absolute value

differentiates the time-varying signal, then finds the point of 0 derivative, and then

converts this point to a TTL signal pulse.
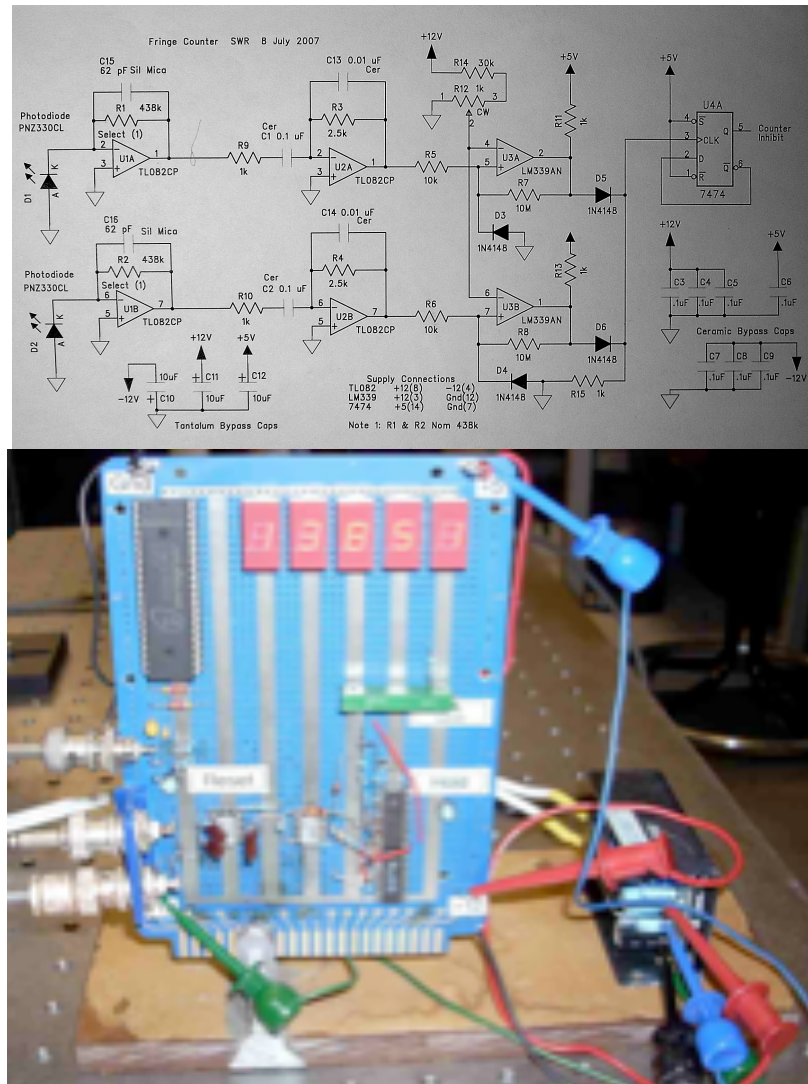
Figure 3.5: Circuit that converts crossing sensors into a start and stop trigger for the counter integrated circuit (large IC on upper left of board). Top: circuit design by Steve Roberts; bottom: implementation of that circuit.

Ideally if the circuit is introducing some error to the timing of this pulse, it will do

so equally for both signals such that any relative error is effectively subtracted. The first

TTL pulse instructs the counter IC to begin counting rising edges of the interference

fringe signal, while the second instructs the IC to stop counting (figure 3.6). The count

value is then displayed with LED's for a visual recording (figure 3.5 shows the actual

circuit board and LED display).
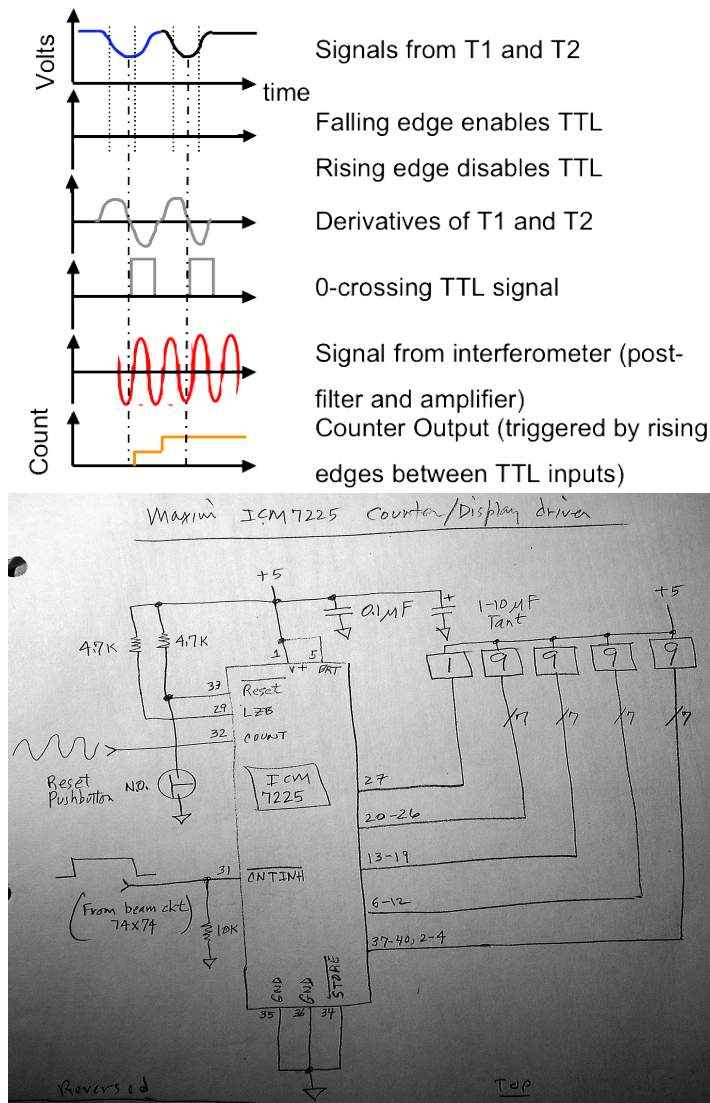
Figure 3.6: Functioning of the crossing sensors. The top figure is a cartoon showing the operations performed by the amplifier (figure 3.5) and counter (bottom). Crossing sensor signals are used to trigger the start and stop of fringe counting, effectively making a real-time comparison between the fringe count and crossing sensors. Both circuit diagrams were drawn by Steve Roberts. Note that falling edges enabled the TTL signal, while rising edges disabled it, such that a null signal doesn't induce a TTL output.

So in summary, when a target maximally occludes the first crossing sensor beam,

a circuit converts this into a "start count" signal; when the target travels to and maximally

occludes the second beam, the same circuit converts this to a "stop count" signal.
Therefore, the crossing sensor beams act as a reference distance that fringe counts can be
compared with.

A test of this mechanism, independent of the fringe count interferometer, was
performed in which a simulated fringe-count signal was input to the counter—in this case
the sinusoidal output from a signal generator (1 MHz ±100 Hz) while 750 kHz is
approximately the maximum fringe count frequency expected in the true experiment.
This signal was then counted as the target passed through the crossing sensors
(effectively timing how long it takes the target to pass through). After 56 repetitions, the
average count was 19657 with a standard deviation of 10.8, indicating that the error in
repeatability was about 5/10000 (figure 3.6). Multiply this by the target drop distance of 1
cm, and the drop repeatability is about 5 μm. Although the error contributions due to each
sub-system are unknown in general, the total error is really what matters in this
demonstration—all that matters is how accurately the fringe count measurement can be
compared with an independent measurement. Since the crossing sensor/trigger system
seemed to perform as desired, further improvements were not pursued, even though there
are ways to improve the crossing sensor developed here.

Target drop timing via 1 MHz sine wave
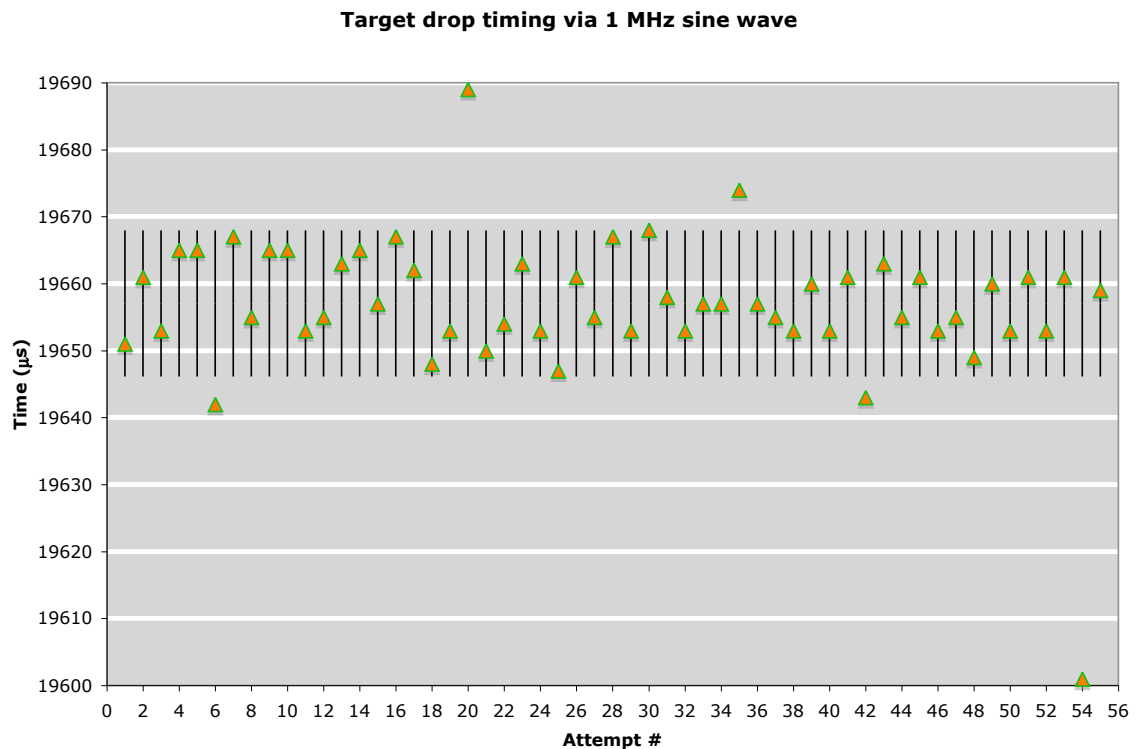
Figure 3.7: Target drop timing measurement results. A 1 MHz sinusoidal signal was input into the counter; then targets were dropped through the crossing sensors. Standard deviation of the resulting data is 10.8 μs, displayed as vertical bars centered on the average, and corresponding to 0.05%.

3.3. Setup: Interferometer

The interferometer is not much different from that presented in (Spalding, Tillack and Carlson); the design is the same as that in figure 2.4, a basic Michelson interferometer with an iris, lens, and spherical (4 mm diameter) mirrored target.

A three-axis stage supports the target dropper, around 20 cm above an optical table (figure 3.8). A mirror reflects the sensing arm of the interferometer 90 degrees, from horizontal to vertical, and is painstakingly aligned to be parallel to gravity so that the target stays well aligned with the interferometer iris, and central Gaussian intensity peak, while it is falling. The alignment process is iterative in nature, as the target dropper

needs to be aligned with the crossing sensor focal plane before the interferometer beam can be aligned with gravity and the target dropper.

The laser diode was set to operate at 63 mW, and 1539.75 nm wavelength; the Gaussian beam was collimated to 16 mm diameter ($1/e^2$) before entering a non-polarizing pellicle (coated nitrocellulose membrane) beam splitter. On first pass, 45% of the light is reflected to a mirror, while 55% is transmitted to the steel target. The T/R ratio may have varied in practice, since the beam splitter is somewhat sensitive to polarization (the author was unaware of this fact during demonstrations, and only discovered this after directly contacting the manufacturer). The light from the mirror and sphere is split once again by the beam splitter, and recombines with the reference light as it passes through an iris set approximately[*] at the central fringe spot diameter. A lens then focuses the light onto a 100 μm amplified InGaAs photodiode (New Focus 2117). The lens and iris were mounted together and attached to a precision 3-axis stage (hand adjusted). The photodiode was also mounted on a precision 3-axis hand-adjustable stage, and aligned with the lens focal point.

To protect the beam turning mirror, an anti-reflection coated window is mounted at a slight angle above the mirror to deflect targets as they fall. While the cost of the window is comparable with that of the mirror (i.e. why not let the target hit the mirror?) the mirror would deflect the target directly into the beam splitter—which in this case was

---

[*] Since the iris was imprecise at such small diameters, ~1 mm, it was simply adjusted by hand until the peak to peak signal was maximized.

a very delicate membrane[*]. Minimal damage to the window's surface coating was

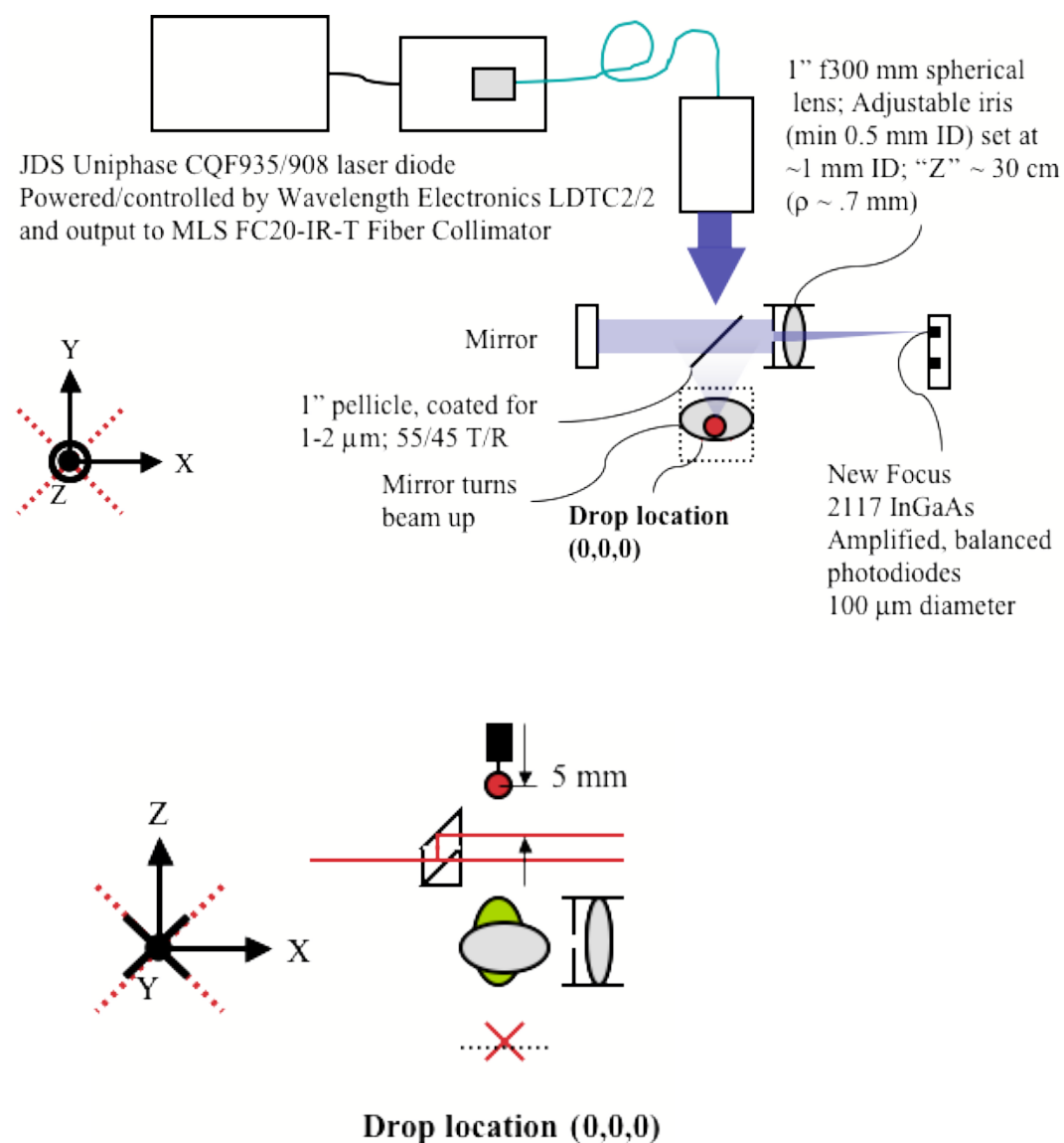observed after numerous drops.

Figure 3.8: Interferometer setup showing all major components. The first diagram is an above view, and the second is a side view (as indicated by the orientation of the (X,Y,Z) axes). See text for details on the laser and detector.

---

[*] The window still caused some undesirable back-reflection/interference since the faces were parallel—a wedged window would be ideal.

The pellicle beam splitter was selected as an alternative to a cube beam splitter, as way to prevent ghosting and secondary interference patterns. However it was found to react to acoustic vibration, which is an undesirable trait for this application. For future applications, it is suggested to resolve both problems by implementing a wedged, AR-coated plate beam splitter. The wedge and AR-coating reduce back-reflections and interference, while the thicker glass material resists acoustic vibrations.

The laser has several relevant stability characteristics (JDS Uniphase): Long term wavelength drift of 0.2 nm, which indicates that the laser can provide long-term wavelength stability of $1x10^{-4}$. This is not sufficient for scenario 1, but is adequate for scenario 2 (and for this demonstration, since the distance being measured is 1 cm; 10 µm/ 1 cm = $1x10^{-4}$). It has low relative intensity noise: -160 dB/Hz from 20-1000 MHz (no value reported under 20 MHz). If this figure is valid at frequencies of interest, the noise would be 6 pW.

The New Focus 2117 detector is (besides a bargain at $1250) relatively high performance (values from spec sheet). It has low dark current, relative to other amplified diodes, of ~2 pW/√Hz. It has a high range of gain values, adjustable from 63X to $1.9x10^{6}$X (bandwidth decreases as gain is increased). It has a range of built-in, 6 dB per octave band-pass filters (where the 3 dB point defines the setting), as well as two matched, balanced diodes. These features, and ease of operation, made it a good choice for the circumstances, although a custom system would be ideal.

In addition to the detector's built-in, adjustable amplifier and filter, an old Tektronix 502 adjustable amplifier/filter was used to add more amplification and filtering capability. Combined, the two filter/amps enabled this demonstration to be carried out;

however, the Tektronix filter was several decades old and introduced additional noise into the signal—estimated to be at least a factor of 5 over that of the detector. The filter roll-off was similar to that for the photodetector—i.e. about 6 dB/octave.

Several attempts were made to take advantage of the detector's signal subtraction capability (as covered in section 2.7) to reduce what seemed to be laser intensity noise (see section 3.5); however this was deemed ineffective with the currently available hardware.

3.4. Demonstration Results

During the final demonstration, a simple set of electronic signal filters and amplifiers was used to make the noisy interferometer output countable with the particular IC. The target was released at 0 elevation, and allowed to fall until about -2 cm; from the -0.5 to -1.5 cm heights, the target was tracked with the interferometer—resulting in counting rates of 0.3 to 0.7 MHz. This set the desired band pass. The Tektronix filters were then set for a band pass between 10 kHz and 1 MHz (closest it could go), while the detector was set for a band between 300 kHz and 1 MHz (also closest it could go to the desired band).

During a series of 53 target drops in which the interferometer signal was counted, the resulting distance measurement was found to be 9.9135 mm with standard deviation 0.0043 mm, after removing the 2 most obvious outlier values. Including the outliers, the values are 9.957 and 0.140 mm, respectively. See figures 3.9 and 3.10 for graphical representations of the data.

Immediately after performing the drop tests, the crossing sensor beam separation distance was re-measured using the methods outlined in section 3.2, resulting in a set of

10 measurements with 9.9765 mm average and standard deviation of 0.005 mm. The results disagree by about 60 μm; this seemingly systematic error has been difficult to explain. The most likely explanation is that the crossing sensor calibration method does not accurately measure the positions at which the target motion results in a start and stop signal. Another explanation is that laser feedback destabilized the laser wavelength (see section 3.5).

When this experiment was attempted at subsequent dates, after a deconstruction and reconstruction of the optical system, it was no longer possible to obtain a countable signal, a fact which indicates the need to improve the design.

Fringe count measurements
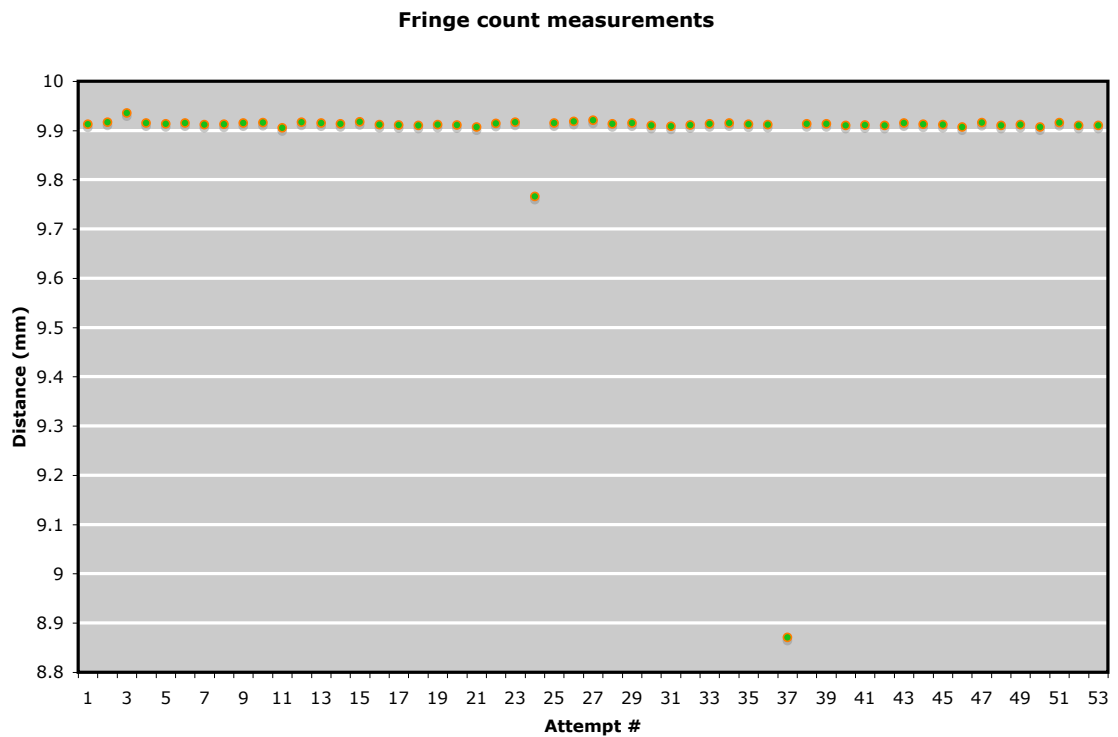
Figure 3.9: Fringe count measurements of a target dropped about 1 cm; 53 measurements resulted in an average distance of 9.957 ±0.14 mm. The information was originally recorded as a number of counts, so the count has been multiplied by λ/2 to get distance. Note that two values are outliers.

Fringe Count Measurements (minus two outliers)
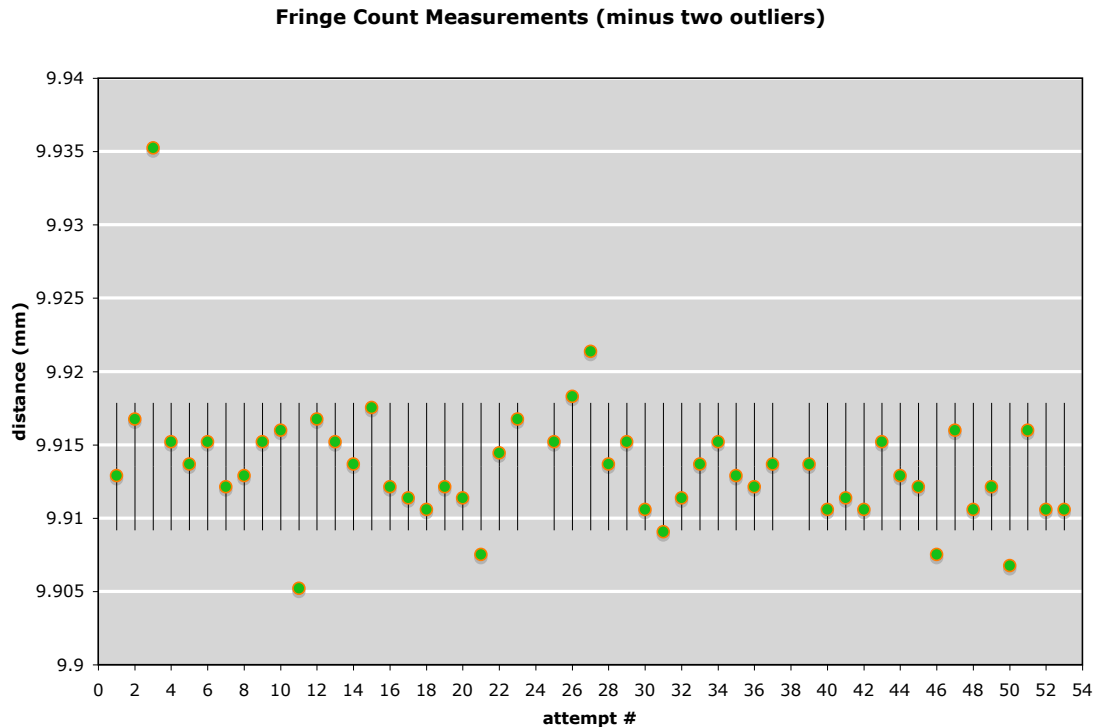
Figure 3.10: Fringe count measurements of a target dropped about 1 cm, with two outliers removed. The average is 9.9135 mm with standard deviation 0.0043 mm (displayed as vertical bars centered on the average value).

3.5. Errors, Noise, and Signal Filtering

The error sources are similar to those listed in section 2.7. Some of these topics have been mentioned in previous sections; this section presents solutions. Of particular concern are laser intensity, laser wavelength, crossing sensor error, and interferometer vibration. These sources of error are interrelated with noise and the need for signal filtering. Here we also relate these issues with the results of this demonstration.

Figures 3.11 – 3.13 emphasize the high level of noise output by the interferometer. Figure 3.11 shows the output from the photodetector, along with an FFT of that output; there is a broad spectrum of noise, as expected. Sadly a picture of a reading taken directly from the laser without the interferometer was not saved, but from

personal memory, the noise in figure 3.12 was due entirely to the interferometer; covering one mirror results in a flat, clean output. Figure 3.12 is the output of the interferometer with a mirror, rather than a metal sphere, as a target. The noise amplitude is the same amplitude as the interference resulting from perturbing (touching) the target mirror. As covered in section 3.3, laser intensity and wavelength are very stable with the particular laser used here. However, due to lack of experience, an optical isolator was not used at the laser output (for example, a faraday isolator). This is very much capable of producing optical feedback noise, which occurs when some light from the laser is reflected directly back into it. In (Lang and Kobayashi) it is shown that AlGaAs (as opposed to our GaInAsp) semiconductor injection lasers exhibit complex relationships between light output, wavelength, and input current when light is reflected directly back into the laser. This was confirmed in an email from Dwight Evard, an engineer at JDS Uniphase (see A.1). This effect may be responsible for some of the noise in the signals of figure 3.12 and 3.13. More disconcerting than noise, though, is the possibility that the laser wavelength could be altered by this feedback; and this may be responsible for the measurement discrepancy in the results section. To determine if optical feedback was causing problems, one would have to purchase an isolator and see if it makes a difference. A fiber-connected isolator could potentially reduce the effect considerably (for instance, http://www.thorlabs.com/NewGroupPage9.cfm?ObjectGroup_ID=3084); alternatively, using the interferometer design with a polarizing beam splitter and $\lambda/4$ plates could solve the problem (while also making better use of laser power).

The crossing sensors are a key component of this demonstration, as well as the overall IFE tracking system (for scenario 1). One weakness of the crossing sensors here is

the method for calibrating them. It was inherently one-dimensional, since a single pinhole was used to represent a dynamic 3 dimensional system. A more advanced camera-based (for example, using NI Vision software) system would be ideal—such that 2-D beam properties, such as intensity distribution at different positions, could be measured. Another area that could be improved is reducing beam focal thickness; if the beams are thin enough, one doesn't need too precise of a characterization to get good results. As used in the demonstration, the beams were about 100 μm thick ($\sim 1/e^2$) at minimum, and up to 20% thicker ±3 mm beyond the focal plane.

If the effective f/# (i.e. f/D) of the beam was below ~5, and the optical layout was designed more carefully (including aspherical lenses), it might be possible to get the crossing sensor focal line thickness down to ~5 μm. The effective f/# in the demonstration was ~20, and spherical lenses were used which further restrict the minimum focal size. For such an improved system, the depth of focus (defined as the region where the spot diameter is below ~5 μm) would need to be at least the target diameter, or ~5 mm (unless smaller targets are used). These are significant challenges for a crossing sensor; if this demonstration were to be duplicated with more advanced hardware, vastly improved performance could be expected. Beyond improving on the crossing sensor designed here would be to replace it entirely with one based on the Poisson spot effect, since the Poisson spot is naturally small in diameter at close range (Petzoldt, Alexander and Carlson). Finally, replacing the laser with a highly stabilized version would also improve performance.

To wrap up the discussion of crossing sensor weaknesses: if the crossing sensors were responsible for the 60 μm error, it would be due to the 3-D nature of the beams combined with the 4 mm diameter target and low-tech calibration methodology.
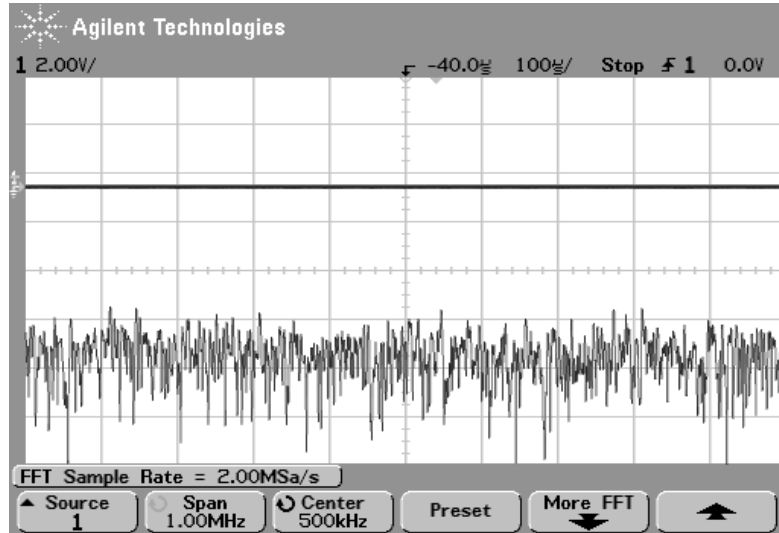

Figure 3.11: Photodetector output with no light input. Noise has even distribution as advertised (upper trace is voltage output; lower trace is FFT spanning 1 MHz).
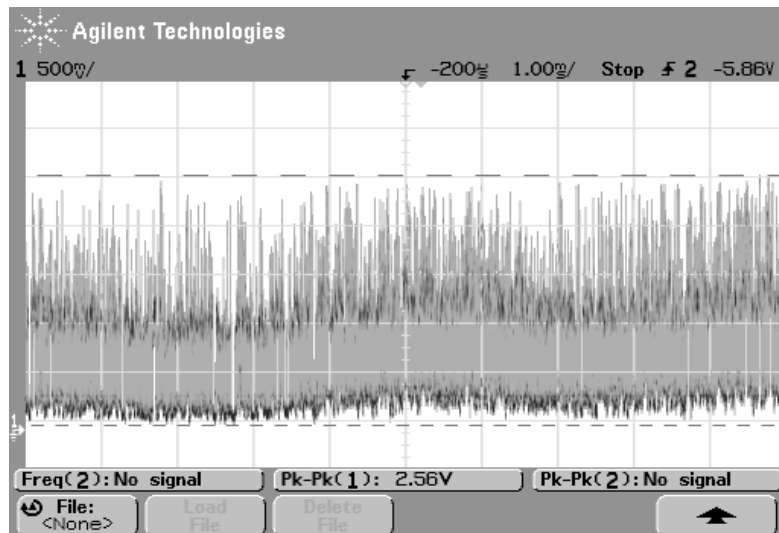
Figure 3.12: Interferometer output signal with no target motion or signal filtering. The dashed lines indicate the maximum voltage swing. The target was a mirror, not a metal sphere.
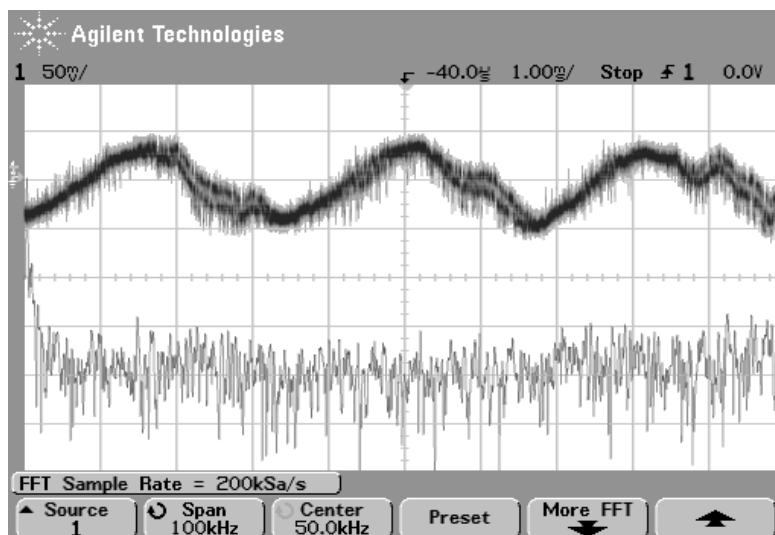
Figure 3.13: Output with filtering, amplification, and a metal spherical target. The target was moved using a hand translator to generate the upper trace. FFT shows broadband noise as well as the ~300 Hz signal.

Interferometer vibrations are a major source of low frequency noise, especially when using a pellicle beam splitter. From a personal conversation with Lane Carlson at GA, the pellicle may be vibrating with amplitude as high as 10 μm due to sound waves. However, the pellicle vibration would be responsible for extra fringe counts, not less, where the results here came up short of what was expected. So this rules out vibration as the source of error. Regardless, using a more stable beam splitter is desirable as mentioned in section 3.3. It would also be ideal to have mechanical isolators keep the interferometer from moving (at least, in the full scale system). The most likely source of noise in the figures above is mechanical vibration, since this is pervasive to the laboratory work environment (and can even be observed due to speaking or making other noise near the interferometer). Some solutions to this issue include placing the system in vacuum, replacing the pellicle with a wedged plate beamsplitter, and/or embedding all interferometer components in optical substrate.

In order to enhance the signal that is a result of target motion, a bandpass filter with pass band between 350 and 750 kHz was desired to replace or augment the low-quality filters used in the demonstration. A filter with as high order cutoffs (low transition widths) as possible was desired; after a few attempts at designing and constructing a one-off filter, it was found that one could be purchased from a professional filter company (TTE company quoted $500 for a 10th order filter—see A.1). A new electronic filter may have enabled better system robustness, but would likely not repair the 60 μm systematic error.

Three separate improvements were needed to be corrected, each requiring the purchase of new hardware; $500 for an electronic filter, perhaps $500 for purchase and installation of a fiber isolator[*], and unknown money to reconstruct and characterize the crossing sensor, since it requires a camera and computer system in addition to a stabilized laser and optics. These improvements would have greatly exceeded the original budget.

---

[*] for instance, http://www.thorlabs.com/thorProduct.cfm?partNumber=IO-H-1550APC

4. CONCLUSIONS

Homodyne fringe counting is a simple concept for tracking IFE targets, and has led to the present state of development. Our initial testing has demonstrated results that hint at the accuracy and precision requirements for IFE, but also reveal robustness issues. A number of developments have come about as a result of this demonstration, including a novel target dropper, and a novel method of verifying tracking performance. Improved signal filtering systems and development of wave-front compensators can most likely improve performance for large-scale systems. Improvements to the demonstration are included.

4.1. Introductory Literature Review

IFE target tracking can glean knowledge and expertise from outside projects, including the LIGO consortium. The literature review performed for this project covered the tip of the iceberg of optical systems, so there is much to be learned and gained from the field. There are also a lot of non-optics fields of research that have developed one-off systems for diagnosing various systems. Assuming that future development of IFE systems will require a large pool of talent in large-scale, precision optics, it is suggested that experts in other fields might be recruited.

4.2. Analysis and Design

A. It was determined that Scenario 1, in which fringe counting is used to measure net distance the target travels from a crossing sensor, requires < 1 ppm precision. It also creates very real problems for receiver design, which may be solvable, since light wavefront radius changes during flight. On the other hand, scenario 2 only measures target velocity during ~1 cm segment of target travel ~10 cm before chamber center.

This enables use of a simple stationary iris and a greatly relaxed < 100 ppm precision. Scenario 2 also reduces the effects of target out-of-round, eliminating the need for target spin in relation to fringe counting.

B. Spherical wave-fronts can be accommodated using a variety of adaptive optical systems, including a simple mechanical lens/mirror, a deformable mirror, an LCD bull's-eye, or an LC-SLM system. The LCD bull's-eye is considered the cheapest, easiest solution.

D. Some sources of error are non-issues for fringe counting--including laser wavelength stability, counter speed, and count resolution. Other error sources are potentially serious, and must be dealt with—including target radius, target out-of-round and crossing sensor precision/accuracy (or equivalently, Glint system performance). Target radius variation must be dealt with by measuring targets in-situ if uniformity cannot be guaranteed; target out-of-round must be compensated for by target spin rates of >1 kHz for scenario 1, and < 250 Hz for scenario 2. Errors introduced via vibration, i.e. time-varying relative positions of interferometer components, can be eliminated by joining all components into a single, thermally stabilized block of optical material, and by isolating this block from the fusion reactor chamber.

4.3 Demonstration

A. A simple, one-off electromagnetic device was designed, built, and demonstrated to reliably and quickly drop steel targets with high accuracy and precision; this design is documented for future efforts.

B. A novel crossing sensor and triggering mechanism, capable of evaluating fringe count tracking system performance, was developed and tested to meet the

precision requirements of scenario 2. Difficulties associated with focus size can be minimized with optimum optical design and a more stable laser, along with updated diagnostics.

C. Interferometer design can be improved by utilizing a faraday isolator to prevent feedback to the diode laser, if not replacement of the homodyne system with a heterodyne system, such as a Zeeman-laser interferometer. The use of a pellicle beam-splitter should be avoided in noisy environments; a wedged plate beam splitter is indicated as a replacement. Signal subtraction was ineffective with the available hardware, and may not be worthwhile in general for this application; however signal normalization is worth development.

D. The best result was a single data set of 53 measurements with a standard deviation of 0.14 mm. When 2 outliers are removed from this set, the standard deviation drops to 0.0043 mm, which is below the required precision for IFE. However, these precise results disagreed with the crossing sensor verification by 0.060 mm, most likely because focal spot diameter of the crossing sensor was nearly 0.2 mm and the beams were not adequately characterized in three dimensions. Also, the single data set could not be repeated on subsequent re-alignments of the interferometer—indicating the sensitivity of the setup and need for improvement in signal filtering and noise reduction.

E. Signal filtering could be improved greatly through use of a high-order band-pass filter (perhaps 10th order). Error in the demonstration could be greatly reduced by better characterizing and improving the design of the crossing sensor mechanism. An optical isolator may improve laser stability.

4.4. An Initial Full System Design

Based on all of this analysis, research, and testing, one can attempt to design a full-scale system before the subsystems have been developed. The first design iteration presented in figure 4.1 may be valuable as an exercise or example of future directions to take.
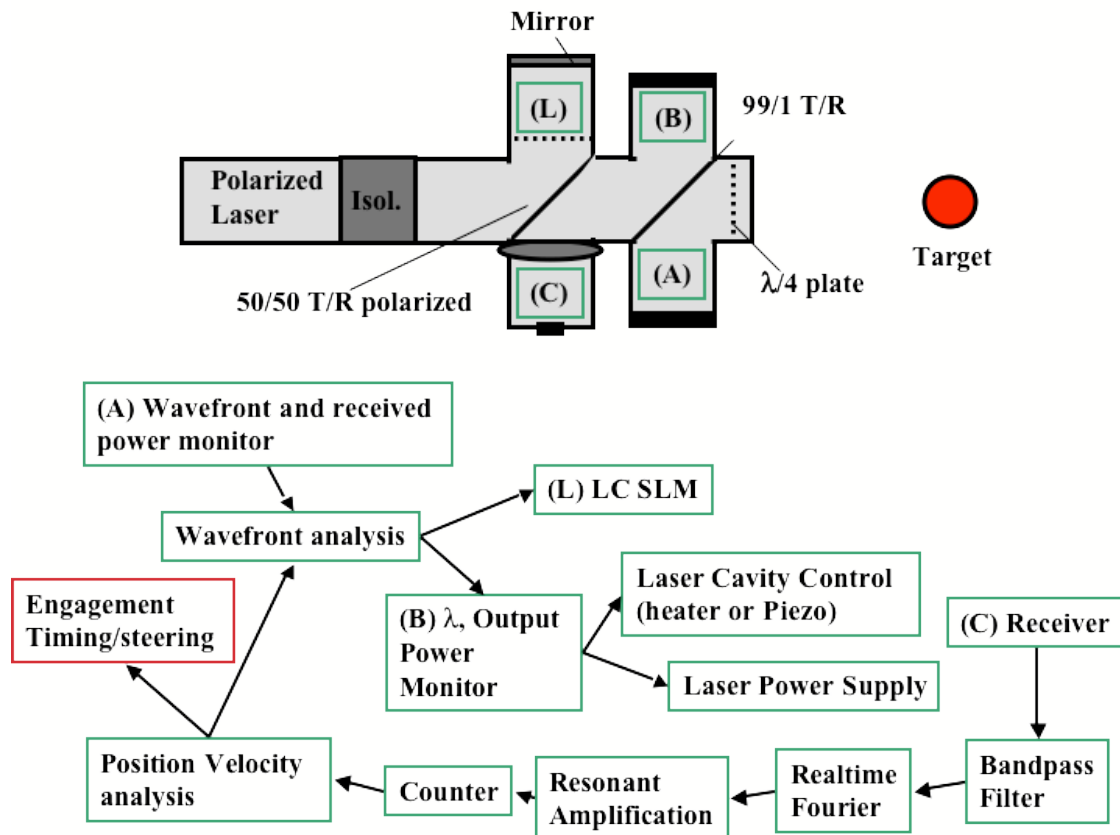
Figure 4.1: A rough, first iteration of a complete system design. Slight variations would exist between scenario 1 and 2 designs. All interferometer components are joined into a single block of optical material to eliminate vibrational noise. A polarized laser and quarter-wave plates enable better use of laser power, or use of a Zeeman-laser (heterodyne) system. All components are integrated in a custom manner, with graded index of refraction coatings used to reduce unwanted secondary reflections. The block diagram shows roughly the direction of information flow.

APPENDIX

A.1 Email Correspondence

Email with TTE, maker of electronic signal filters
> -----Original Message-----
> From: Dave [mailto:dzavac@tte.com]
> Sent: Thursday, January 10, 2008 10:31 AM
> To: jdspaldi@hotmail.com
> Cc: Jennifer Gilmore
> Subject: TTE Verbal Quote / Simulations - UCSD - Jon Spaulding (1-10-07)
>
> RE: TTE Speed Quote: he1182-350k-bnc-720b
>
> Good morning Jon,
>
> Thanks for your inquiry and interest in TTE filters. We appreciate it.
>
> Based on your requirement below this is what we can offer - let me know if works for
> you.
>
> -0.7dBc at 400kHz
> -3dBc at 350kHz
> -80dBc at 291kHz
> 50 ohms
> BNC Female Connectors
> Case 720B
>
> Delivery at one (1) week ARO
> Price at $423.00 each for one (1) to nine (9) units.
>
> Simulations attached and a special part would need to be assigned prior to order.
>
> Please let me know if you have questions, comments or need any additional
information
> or assistance.
>
> Best regards,
>
> Dave
> _____
>
> David Zavac
> Sales Manager
>

> TTE, Incorporated
> East Coast Sales Office
> 6295 Gulf Blvd., Suite 9
> St. Pete Beach, FL 33706
>
> 1-866-363-0849 (Toll Free)
> 1-727-363-0849 (Local)
> 1-727-363-7639 (Fax)
>
> dzavac@tte.com (Email address)
> www.tte.com (Web address)
>
> -----Original Message-----
> From: sales [mailto:sls@tte.com]
> Sent: Wednesday, January 09, 2008 10:59 AM
> To: dzavac@tte.com
> Subject: FW: TTE Speed Quote: he1182-350k-bnc-720b
>
> -----Original Message-----
> From: jdspaldi@hotmail.com [mailto:jdspaldi@hotmail.com]
> Sent: Wednesday, January 09, 2008 12:45 AM
> To: sales@tte.com
> Subject: TTE Speed Quote: he1182-350k-bnc-720b
>
> name: jon spalding
> TTE Part #: he1182-350k-bnc-720b
> Specification: high pass with 0db attenuation at 400khz, sharp cutoff (i.e.
> high order).
> Specification2:
> Specification3:
> Email: jdspaldi@hotmail.com
> Company: ucsd
> Phone: 661-713-6621

Hi John,

It was a pleasure talking with you this afternoon. Unfortunately I did
not find a good technical reference on noise caused by back reflections
in diode lasers. However, this may well be the cause of the noise that
you are seeing in your system. One option is to use an isolator,
something like the product in the attached datasheet. Optical isolators
are available from other optical comms component vendors as well. Hope
this helps.

Regards,

Dwight

_____

Dwight Evard
Sales Development Manager
JDSU Commercial Lasers
Office: 408-546-4546
Mobile: 408-506-7504

Email correspondence with Hovemere Ltd, makers of precise wavelength measurement systems

yes we can match this accuracy theoretically (although proving it is tricky
as the refractive index change in air results in the wavelength of light
moving of this order if my memory is correct:-)

  We can measure up to 70 Hz, this is limited by the readout time of the
detector.

  mike

-----Original Message-----
From: jdspaldi@ucsd.edu [mailto:jdspaldi@ucsd.edu]
Sent: 03 January 2006 20:33
To: mfoster@hovemere.com
Subject: RE: Absolute wavelength meter

Mike,

For a wavelength range of 300-600 nm, would it be possible to get an
accuracy of +/- 2 fm? Also, out of curiosity, what is limiting the
measurement rate, and can that be increased if necessary?

Thanks again,

Jon
>
> Hi Jon
>
> The price of these systems varies from $ 25,000 USD up to $ 55,000 USD
> depending on a wavelength range , accuracy required etc.
> If you know the wavelength within certain limits to start with we find

> that
> for most applications the relative system is sufficient particular when
> very
> high accuracy is required. This may be better suited to your application.
>   I have attached a spec sheet to provide you with some more detailed
> information about these systems.
>
>   Yours
>
>   Mike
>
> Dr M J Foster
> Lidar Technologies Ltd
> Arctic House
> Dunton Green
> Sevenoaks
> TN 14 5HD
> Tel +44 (0) 1732 469 696
> Fax +44 (0) 1732 469 695
>

The following email correspondence occurred around August 2nd, 2005. Ted Strand
(strand1@llnl.gov) works on a high-speed Doppler velocimeter.

Jon,

When I think of inertial confinement targets, I visualize fairly
small (few mm diameter) objects. Do you really mean that you want to
follow the target shell for a distance of 10 meters?

Our detectors are high-speed (12 GHz) InGaAs detectors that we bought
from Newport Corporation (model AD-40APDir-FC). These are fairly
expensive and we need them only because we want to go to velocities
around 5 km/s. We also need very expensive high-sample-rate (20 GS/s)
digitizers for the same reason. But if you need to measure only 100
m/s, then you can relax those criteria quite a bit and use much less
expensive components. The beat frequency for 100 m/s is only 129 MHz
when using 1550 nm lasers, so you could use much lower bandwidth
detectors and more standard digitizers. Having a low velocity limit
would let you build a much less expensive system than we have.

Ted

>Ted,
>

>Thanks for the response. The target will be moving around 100 m/s for 10
>meters.
>
>What kind of photosensors did you use?
>
>-Jon
>
>> Jon,
>>
>> Sorry I did not respond sooner, but I was on vacation for the past
>> week and a half, and I just returned today. I have enclosed a
>> PowerPoint presentation that I gave at the SPIE conference in
>> Alexandria, VA, this year--hopefully it will answer many of your
>> questions.
>>
>> You asked specifically about the accuracy--I assume you mean the
>> uncertainty in the velocity obtained with this method. I am afraid I
>> cannot give you a simple one-word answer, because the uncertainty
>> depends upon the method of the data analysis. And the method of data
>> analysis depends upon the range of values that you plan to measure.
>> Let me give you a few examples.
>>
>> We generate a beat signal by mixing the doppler-shifted light with
>> some undoppler-shifted light. We obtain a full beat cycle every time
>> the surface moves one-half the wavelength of the laser light, that
>> is, we get a full beat cycle for every 775 nm of motion. We have
>> several ways that we analyze our data.
>>
>> Example 1: If we have an experiment in which we follow a surface
>> moving 1000 m/s for 100 mm, we generate approximately 129,000 beat
>> cycles. In this case, we would analyze the data using a sliding
>> Fourier transform. Our software allows us to choose the number of
>> beat cycles over which to perform each transform. If we choose a
>> Fourier transform window of 65 cycles, then we can usually obtain
>> less than 1% velocity uncertainty, but our time response is over 50
>> ns. If we choose the Fourier transform window to be shorter, say, 8
>> cycles, then we achieve 6 ns time response, but now we obtain 3 - 4%
>> velocity uncertainty. Using the Fourier transform method, there is a
>> (deltaV)(deltaT) product limitation similar to the Heisenberg
>> uncertainty principle--the better we want to know the velocity, the
>> worse we know the time response.
>>
>> Example 2: If we have an experiment in which we follow a surface for
>> only ten microns, regardless of the velocity, we obtain only 12 to 13
>> beat cycles. In this case, we would analyze the data using a sliding

>> sine fit in which the fit is calculated over approximately one cycle.
>> Our temporal resolution is now relatively fixed and the velocity
>> uncertainty varies greatly depending upon the number of points per
>> cycle we obtained with our digitizer and the amount of noise in the
>> data. With 8 to 10 points per cycle and very little noise, we can
>> obtain sub-percent velocity uncertainty. But with 4 or so points per
>> cycle and more noise, we may achieve 5 or 10% uncertainty in the
>> velocity.
>>
>> If you could give me some idea of the velocity and range of motion
>> that your experiment might have, then I could give you a better idea
>> of the velocity uncertainty that you might be able to obtain. I hope
>> this helps.
>>
>> Ted Strand
>>
>>>Ted,
>>>
>>>I am attempting to demonstrate a doppler velocimeter to be used in
>>>Inertial Confinement Fusion, as a means of tracking the target fuel
>>> shell.
>>> I found a report from LLNL about a system you used to measure
> >> velocities
>>>based on beat frequency, and I was wondering if you could give me some
>>>advice on my project. What kind of accuracy did you you get with the
>>>20GHz/1550 nm system you used?
>>>
>>>Thanks for replying,
>>>
>>>Jon Spalding
>>>Summer intern
>>>General Atomics
>>>San Diego, Ca
>>

A.2 Cat's Eye Retro-reflector: Valuable Alignment Tool

Cat's eye is a term given to N=2 spheres, because they reflect a high fraction of

incident light (much like a Cat's eye). N=2 sphere is short-hand for a spherical ball lens

with index of refraction 2. A glass sphere that has an index of refraction 2 acts as a retro-

reflector, returning any signal that enters it in the opposite direction (figure A.1).
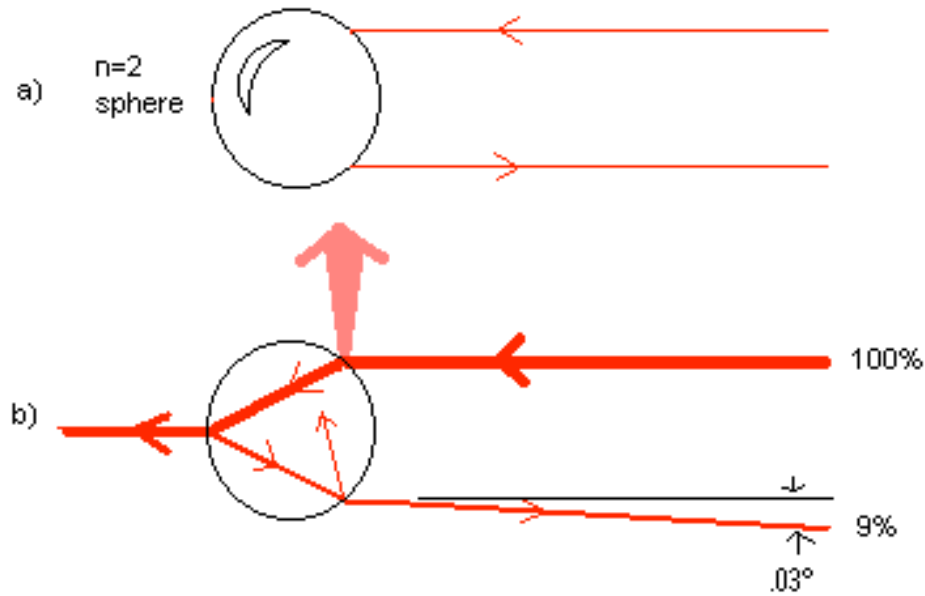
Figure A.1: The retro-reflective capabilities of the N=2 sphere. Sketch a) represents the ideal behavior of a retro-reflector: light comes in, and then is reflected straight back precisely parallel to the incoming beam. Sketch b) shows how the N=2 sphere deviates from an ideal retro-reflector: A fraction of the light that is incident on the sphere is reflected, and the rest enters. The light that enters is bent and hits approximately the exact rear of the sphere, where it is again partially reflected and partially transmitted. The reflection then leaves the sphere at the opposite side from where it entered (again, partially transmitted and partially reflected). Approximately 9% of the light that enters the sphere is reflected; since the sphere has some aberration, the reflected light has some divergence (measured experimentally at .03 degrees for 632.8 nm Helium Neon laser light).

The primary purpose of understanding the N=2 sphere is that it is extremely useful in aligning an interferometer. It reflects almost perfectly anti-parallel to any incoming beam of light—which is convenient for aligning photodiodes, mirrors, and beamsplitters.

A second purpose of studying the N=2 sphere is that it may be used in scaled up tracking demonstrations; since it reflects about 9% of incident light, it reduces laser power requirements vs. the levels required for tracking a metal sphere of the same size, meanwhile eliminating the need for an iris. While performance of this sphere is not as

good as a corner cube retro-reflector (which is 100% rather than 9% efficient), it is very cheap and simple to mount, it doesn't require any alignment, and it reflects light coming from any direction (over 4π steradians), unlike a corner cube that must be facing the incoming light. A limitation is that the relative index of refraction, and hence reflection properties, vary for different laser wavelengths—meaning efficiency may be reduced for some wavelengths. Further information on this component and others can be found at: www.slac.stanford.edu/econf/C9910183/papers/045.PDF.

There are subtleties to the N=2 sphere that differ from an ideal retroreflector, besides beam divergence. That is, abnormalities in the reflected wave-front, and interference patterns in the reflected light. See figure A.2 and A.3 below.
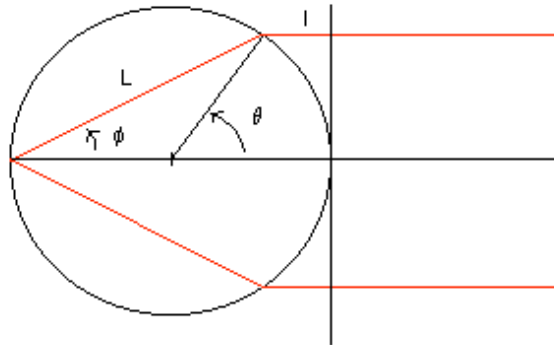

Figure A.2: Angular dependence of reflections from N=2 sphere. The path length of an entering ray depends on its distance from center. Any interferometer images will have ring patterns, and attempts to get a clean signal for counting purposes will be reduced by this fact.

The path length vs. theta dependence is defined as follows, for a sphere of radius R:

$$\phi = \theta / 2$$
$$l = n_{air} R(1 - \cos\theta)$$
$$L = n_{sphere} R \sin\theta / \sin(\theta / 2)$$
$$L_{total} = 2(l + L)$$

Therefore, light reflected from the front surface of the sphere will interfere with light reflected internally. This may then also interact with diffraction of the reflected light.

This formula was applied in an excel spreadsheet, with n_{air} approximated at 1 and n_{sphere} approximated at 2 (actual values vary slightly, and change with laser wavelength). Next, the angle that corresponds with a path length difference of $\lambda/2$ was solved for, and converted to a spot size. This spot size determines how small the opening of an iris should be, such that signal amplitude is maximized and the central peak in figure A.3 is all that is interfering in the fringe counting interferometer. The spot size is around .4 mm in diameter at the front surface of the (5 mm diameter) sphere, and growing at further distances due to 0.06° divergence.
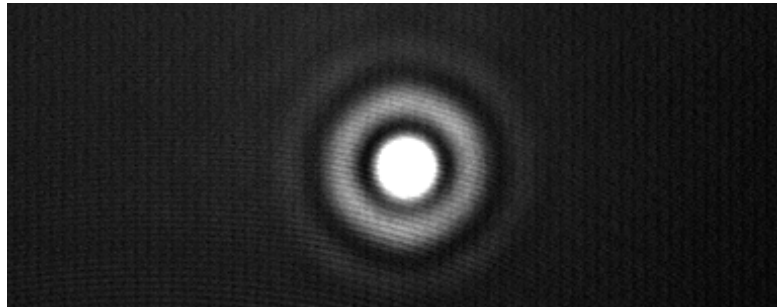

Figure A.3: Overfilled N=2 sphere reflection. Image not to scale—central spot is around .2 mm in diameter. This is not an interference pattern caused by the interferometer, but is inherent to the Cat's Eye. Interference of this reflection with a plane wave is somewhat complex—although, unlike the interference of a point source (spherical wavefront) with a plane wave, this interference results in a net signal amplitude (for the test case of a Gaussian laser beam).

A.3. Proposed Pellet-gun Demonstration

A test was performed that demonstrated the aerodynamic stability of an air-rifle pellet when a glass sphere was glued in the back of the pellet—see figure below. It may

be worthwhile to attempt tracking a retro-reflective pellet such as this with fringe count
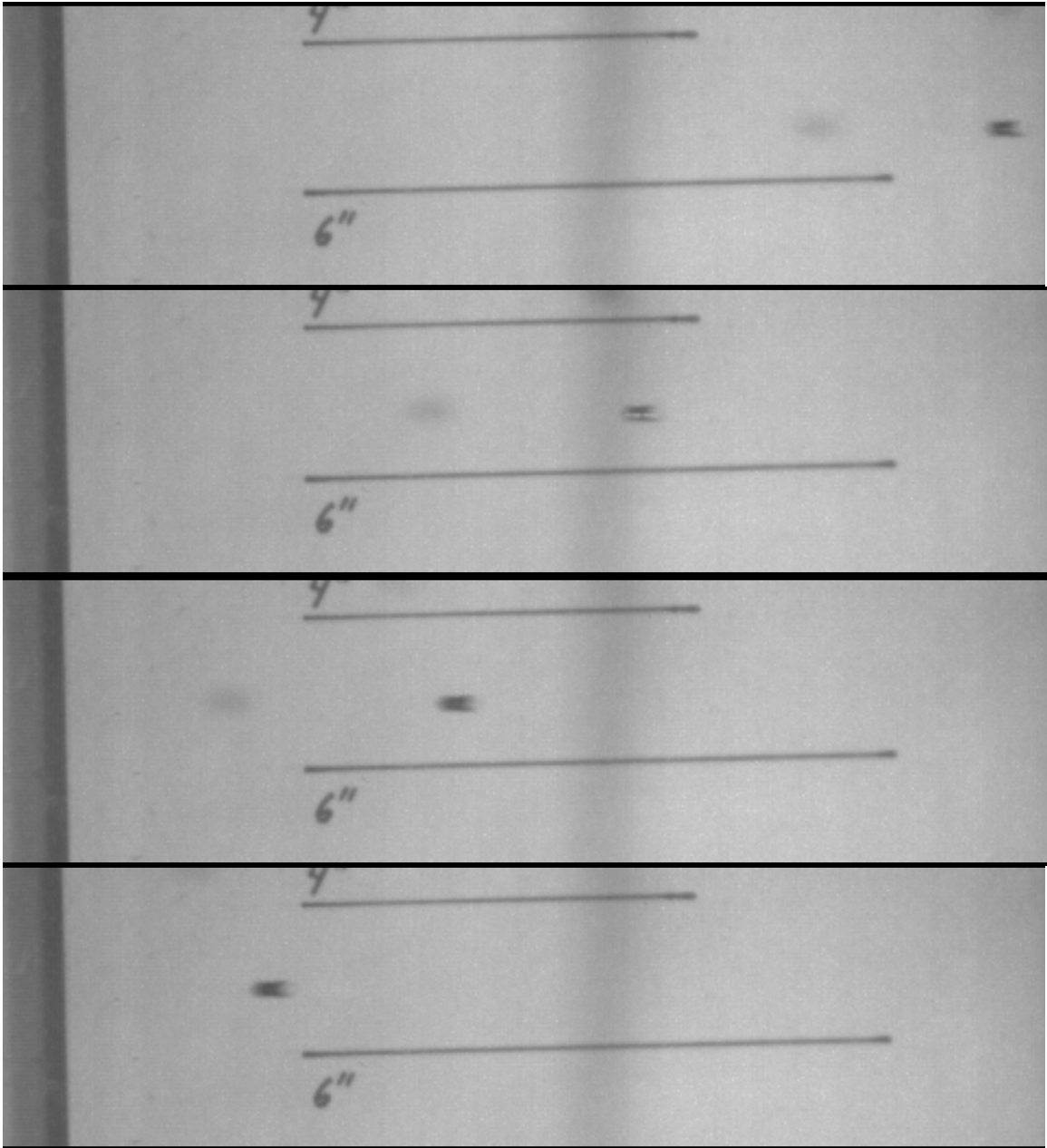
tracking.

Figure A.4: A heavy type of air rifle pellet had a glass sphere (partially visible in these high-speed images) glued in the rear as the pellet was fired from a high-powered air rifle in the injector test facility at GA. The pellet is traveling from right to left (several of the photos were removed for the sake of space).

A high-speed camera was used to obtain images of the pellet/sphere in-flight, and see that it was not flipping or otherwise destabilized. Such a high-speed, large-scale demonstration could be used to cheaply test fringe counter systems, since gluing an N=2 sphere into a pellet enables a strong signal return. Alternatively, a pellet could be modified by cutting or gluing a corner cube into the back end to achieve better light return.

A.4. Heterodyne System: Implementation and Ideas

As discussed in the introduction, there are benefits to using a heterodyne rather than homodyne interferometer. First, heterodyne systems are less sensitive to light intensity fluctuations. Second, heterodyne systems can differentiate between forward and backward motion with no difficulty.

The introduction lays out pretty well how to implement a heterodyne interferometer, except that it skips how one analyses the output from such an interferometer. It also doesn't mention the consequences of the signal frequency exceeding the laser frequency splitting. (Zygo Company) is geared towards applications under 4 m/s, where signal frequencies are two orders of magnitude less than the carrier frequency—making it possible to separate the two. For a 100 m/s target, an extremely high carrier frequency would be desired—on the order of 2 GHz, which requires a laser with two separated wavelength outputs (for instance, 1.50 μm and 1.65 μm). Then the 2 GHz carrier signal could be locked-into to avoid most sources of noise, and the 133 MHz Doppler signal could be measured precisely. Obviously this requires modern electronics.

If lower carrier frequencies are used (such as the 4 to 20 MHz mentioned in (Zygo Company)) there are some options. First, if the low frequency is in the target arm of the

interferometer, and the signal frequency approaches the carrier frequency, the beat frequency can go to zero. If the high frequency is in the target arm of the interferometer, the carrier frequency will be overwhelmed by the signal (which is essentially the same as a homodyne interferometer). So, a Zeeman system could be used to effectively increase or decrease the fringe count signal frequency—target velocity information is present in the net change of the beat frequency from the carrier frequency.

The notion that the heterodyne system could effectively decrease the signal frequency can be extended as follows. If the carrier frequency is nearly the same as the Doppler shift, the beat frequency can go to 0 (as mentioned above). This fact could be used as the method of measuring target velocity, assuming one can very precisely determine the laser output frequencies. In order to keep the Doppler shift and carrier frequencies very closely matched, a feedback would be used to adjust the magnetic field, and hence frequency output, of the laser. Figure A.5 outlines this idea, labeled a "Null Zeeman interferometer." A very precise wave-meter would be needed to operate in real time (sub ms); these are available (see email from Hovemere in A.1).
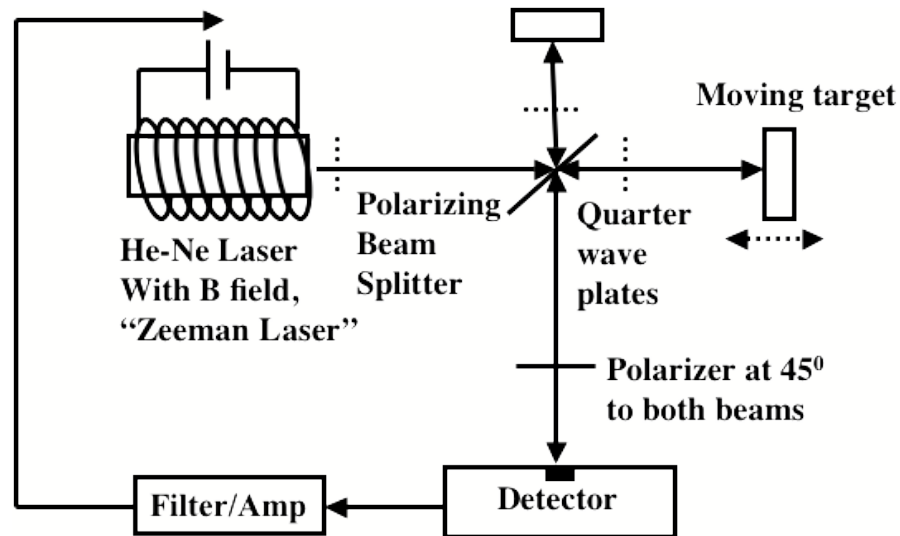
Figure A.5: Null Zeeman interferometer concept. When the Zeeman frequency shift is equal and opposite to the Doppler shift of the light returning from the target (i.e. for a target moving away from the interferometer, the target beam has a higher frequency than the reference beam and vice-versa), the detector will measure a constant output (ignoring non-ideal effects on laser intensity); therefore the detector output can be used to control the Zeeman shift to null the target signal. Then the wavelength of the shifted light needs to be measured very precisely to determine target velocity—the Doppler shift would be measured by comparing the two laser output wavelengths. A similar system could be used with an acousto-optic modulator, since those are also controlled electronically.

Now, sadly, a heterodyne system will not address the problem of spherical wave-fronts, even if the system is setup to have a extremely low frequency beat signal. This is because the wavelength of the return signal is essentially the same regardless of the beat frequency. Increasing laser wavelength is the only way to enlarge the spatial extent of the bull's-eye fringe pattern (in the process increasing lateral robustness and reducing the need for an iris). So the iris or other compensators mentioned in chapter 2 would still be desired with a heterodyne system using near-visible wavelengths.

REFERENCES

Barker, L M and R E Hollenbach. "Shock-Wave Studies of PMMA, Fused Silica, and Sapphire." Journal of Applied Physics 41.10 (1970).

Barker, L M and R E Hollenback. "Laser Interferometer for Measuring High Velocities of any Reflecting Surface." Journal of Applied Physics 43.11 (1972).

Carlson, L, et al. "Target Tracking and Engagement for Inertial Fusion Energy - A Tabletop Demonstration." Fusion Science and Technology 52.3 (2007): 478-482.

Dahlquist, J A, D G Peterson and W Culshaw. "Zeeman Laser Interferometer." Applied Physics Letters 9.5 (1966).

Flint, G. Notes Concerning the Injection, Tracking, and Simulation of FTF and IFE Targets. General Atomics. San Diego, 2006.

Halliday, Resnick and Walker. Fundamentals of Physics. 6th Edition. Wiley, 2001.

Hariharan, P. Optical Interferometry. San Diego: Elsevier Academic Press, 2003.

JDS Uniphase. "Product Bulletin: 63 mW 1550 nm CW DFB Lasers with PM Fiber for WDM Applications--CQF935/908 Series." n.d.

Kubota, T, M Nara and T Yshino. "Interferometer for Measuring Displacement and Distance." Optics Letters 12.5 (1987): 310-312.

Lang, R and K Kobayashi. "External Optical Feedback Effects on Semiconductor Injection Laser Properties." IEEE Journal of Quantum Electronics QE-16.3 (1980).

Lawrence Livermore National Laboratory. Inertial Fusion Energy: How IFE Works, NIF & Photon Science. 2008 <https://lasers.llnl.gov/programs/ife/how_ife_works.php>.

LIGO Scientific Collaboration. Detector Description and Performance for the First Coincidence Observations between LIGO and GEO. 2003.

Munro and et. al. "Shock Timing Technique for the National Ignition Facility." Physics of Plasmas 8.5 (2001): 2245.

Murphy, T. Apache Point Observatory Lunar Laser-Ranging Operation. 2007 <http://physics.ucsd.edu/~tmurphy/apollo/apollo.html>.

Petzoldt, R and K Jonestrask. "IFE Target Injection Tracking and Position Prediction Update." Fusion Science and Technology 47.4 (2005): 1126-1130.

Petzoldt, R W. "Wake Effect on Target Trajectory in Air." Memo. General Atomics, 2007.

Petzoldt, R, et al. "A Continuous, In-Chamber Target Tracking and Engagement Approach for Laser Fusion." <u>Fusion Science and Technology</u> 52.3 (2007): 454-458.

Pierrottet, D et. al. "Development of an All-Fiber Coherent Laser Radar for Precision Range and Velocity Measurements." <u>Materials Research Society Symposium Proceedings</u> (2005): 71-78.

Saulson, P R. <u>Fundamentals of Interferometric Gravitational Wave Detectors</u>. Singapore: World Scientific, 1994.

Sethian, J D. "Fusion energy with lasers, direct drive targets, and dry wall chambers." <u>Nuclear Fusion</u> (2003): 1693-1709.

Shirai, T, T H Barnes and T G Haskell. "Adaptive Wave-front Correction by Means of All-Optical Feedback Interferometry." <u>Optics Letters</u> 25.11 (2000): 773.

Spalding, Jon D, et al. "Longitudinal Tracking of Direct Drive Inertial Fusion Targets." <u>Fusion Science and Technology</u> 52.3 (2007): 435-439.

Tillack, M S, et al. "A Target Fabrication and Injection Facility for Laser-IFE." <u>20th Symposium On Fusion Engineering</u>. San Diego: IEEE/NPSS, 2003.

Zygo Company. "A Primer on Displacement Measuring Interferometers." 1999. <www.zygo.com/products/zmi/dmiprim.pdf>.